NASA TECHNICAL NOTE

NASA TN D-5838

c. 1

NASA TN D-5838

SOME TURBULENT BOUNDARY-LAYER MEASUREMENTS OBTAINED FROM THE FOREBODY OF AN AIRPLANE AT MACH NUMBERS UP TO 1.72

by Edwin J. Saltzman and David F. Fisher

Flight Research Center
Edwards, Calif. 93523

NATIONAL AERONAUTICS AND SPACE ADMINISTRATION • WASHINGTON, D. C. • JUNE 1970

1. Report No. NASA TN D-5838	2. Government Accession No.	3. Recipient's Catalog No.
4. Title and Subtitle SOME TURBULENT BOUNDARY-LAYER MEASUREMENTS OBTAINED FROM THE FOREBODY OF AN AIRPLANE AT MACH NUMBERS UP TO 1.72		5. Report Date June 1970 6. Performing Organization Code H-567
7. Author(s) Edwin J. Saltzman and David F. Fisher		8. Performing Organization Report No.
9. Performing Organization Name and Address NASA Flight Research Center P. O. Box 273 Edwards, California 93523		10. Work Unit No. 126-13-02-02-24 11. Contract or Grant No.
12. Sponsoring Agency Name and Address National Aeronautics and Space Administration Washington, D. C. 20546		13. Type of Report and Period Covered Technical Note 14. Sponsoring Agency Code

15. Supplementary Notes

16. Abstract

Boundary-layer-profile data were obtained from the smooth undersurface of an airplane fuselage during the demonstration of sensors for measuring boundary-layer characteristics. The data represent Mach numbers from 0.51 to 1.72, angles of attack up to 7°, and Reynolds numbers up to 74 million. The data are interpreted in terms of local skin friction and momentum thickness, and the velocity profiles from which these data are derived are tabulated.

Local transformed friction coefficients obtained from a Clauser type of determination from velocity profiles were close to the incompressible values of Kármán-Schoenherr when presented as a function of momentum thickness Reynolds number. Turbulent momentum thickness values were significantly influenced by angle of attack. The flight values of momentum thickness for angles of attack near 6° to 7° were lower than flat-plate values, approaching the level for slender cones. At angles of attack near 0° to 1°, momentum thickness from flight was higher than flat-plate values. The aircraft nose boom and the protuberances on the boom are believed to be major reasons for the additional thickness at low angles of attack.

17. Key Words Suggested by Author(s)	18. Distribution Statement
Skin friction - Turbulent boundary layer - Protuberances	Unclassified - Unlimited

19. Security Classif. (of this report)	20. Security Classif. (of this page)	21. No. of Pages	22. Price*
Unclassified	Unclassified	45	$3.00

*For sale by the Clearinghouse for Federal Scientific and Technical Information, Springfield, Virginia 22151

SOME TURBULENT BOUNDARY-LAYER MEASUREMENTS OBTAINED FROM THE FOREBODY OF AN AIRPLANE AT MACH NUMBERS UP TO 1.72

Edwin J. Saltzman and David F. Fisher
Flight Research Center

INTRODUCTION

Because the skin-friction drag of a large aircraft is a significant portion of the total cruise drag, it is important to develop an accurate understanding of skin friction and the associated boundary-layer characteristics of large configurations under real environmental conditions. When comparing aerodynamic parameters obtained from full-scale flight to corresponding data from ground facilities, it is desirable to eliminate differences in experimental techniques which can add variables to the comparison. Thus, it would be helpful if some of the techniques used for wind-tunnel boundary-layer studies could be adapted to full-scale flight investigations.

The NASA Flight Research Center has studied means of using, in a full-scale flight environment, some of the techniques which have been successful in ground facility studies. A brief review of these techniques shows that skin-friction studies usually followed one of two general approaches: direct force measurements or definition of pressure losses in the flow. Reference 1 compiles the results of several early force-measurement studies for incompressible flow (including towed planks in water), and reference 2 discusses early studies of incompressible flow pressure losses in pipes.

In recent years, both the force-measurement approach and various boundary-layer-analysis methods, for example, pressure loss, have been improved. Compact and relatively accurate friction-force gages have been developed, first for use in wind tunnels (refs. 3 to 7), and later for use in flight (refs. 8 and 9). The boundary-layer-analysis methods range from the surface impact-probe technique of Preston[1] (ref. 11) to the detailed profile analysis of boundary layers in wind tunnels, such as reported in references 4, 6, and 12 to 15. Some of the most meaningful boundary-layer information has come from studies such as these, because the boundary layer can be examined in considerable detail in a wind tunnel where flow conditions can be closely controlled. However, the otherwise comprehensive wind-tunnel studies are usually limited by small scale and lower Reynolds numbers, relative to a real, full-scale flight environment.

The purpose of the work which led to this paper was to demonstrate in flight the integrity of several elements of a boundary-layer complex. The paper was prepared because, in retrospect, it was thought that the relatively high Reynolds numbers and the

[1]Preston's technique of evaluating local friction was adapted for use on flat-plate compressible flow and used by numerous experimenters. The comprehensive work of Hopkins and Keener (ref. 10) summarizes the literature on surface impact probes and provides a calibration for compressible flow.

angle-of-attack effects obtained in the demonstration would be of interest to other investigators. The paper presents, primarily, boundary-layer-profile data obtained from the bottom surface of the fuselage of a supersonic Navy airplane, the A5A. The data represent level flight over a Mach number range from 0.51 to 1.72 and Reynolds numbers up to 74×10^6, based upon an assumed length of turbulent flow (from the nose apex to the boundary-layer complex). The data presented are interpreted as skin-friction coefficients derived from the boundary-layer measurements and some generally used expressions of boundary-layer thickness. Comparisons are made with the incompressible friction levels of the Kármán-Schoenherr formulation and flight friction values obtained by French researchers from the delta wing of a supersonic airplane.

SYMBOLS

a	distance rearward from fuselage nose apex (fig. 5)
b	distance from fuselage nose apex to juncture of fuselage and wing leading edge (fig. 5)
C_F	average friction coefficient for flat plate, $\frac{2\theta}{x}$
C_f	local friction coefficient, $\frac{\tau}{q}$
C_p	pressure coefficient, $\frac{(p_{local} - p_\infty)}{q_\infty}$
H	boundary-layer-shape factor, $\frac{\delta^*}{\theta}$
l	axial distance from nose apex to boundary-layer-complex fuselage station
M	Mach number
n	profile index, as in $\frac{u}{u_1} = \left(\frac{y}{\delta}\right)^{1/n}$
p	static pressure
$\frac{dp}{dl}$	variation of static-pressure in axial direction
q	dynamic pressure, $\frac{\gamma}{2}M^2p$
R_x	Reynolds number based on dimension x
R_θ	Reynolds number based on momentum thickness θ
T	static temperature, local value unless subscript or superscript used

T_s stagnation temperature

T' reference temperature, as in reference 19

u local velocity

u_τ friction velocity, $\left(\frac{\tau}{\rho'}\right)^{1/2}$, where ρ' is based on T' temperature, as defined in reference 19

x assumed distance from virtual origin of turbulent boundary layer[2]

y distance from the surface

z vertical distance from waterline reference plane (which passes horizontally through the nose boom) to bottom surface of the fuselage at the airplane centerline

α indicated airplane angle of attack

γ ratio of specific heats, 1.4

δ boundary-layer thickness

δ^* displacement thickness of boundary layer

θ momentum thickness of boundary layer

μ absolute viscosity

ν kinematic viscosity

ρ density, local value unless subscript or superscript used

τ surface friction stress

$'$ based on reference temperature T'

$\bar{}$ over a quantity denotes flat plate and zero longitudinal pressure gradient

$\frown$ over a quantity indicates a curved surface

Subscripts:

f flight, from present study

i incompressible, M = 0

max maximum

[2]The assumed value of x for transition at the nose apex is 200 inches (508 centimeters). If it is assumed that transition occurred near the tip of the nose boom, the value of x used is 290 inches (736 centimeters).

pp	Preston probe
r	rake
t	theoretical
tp	traversing probe
1	conditions at edge of boundary layer
∞	free-stream conditions

TEST FACILITY AND CONDITIONS

The demonstration of the boundary-layer-rake complex required an aerodynamically clean surface. The bottom centerline of an available aircraft, the A5A, was chosen because it had a smooth contour and was free of adjacent protuberances or gaps. A brief description of the airplane is presented in reference 16, which discusses the primary mission of this airplane at the NASA Flight Research Center. A photograph of the airplane is shown in figure 1. A drawing is presented in figure 2 which shows the location of the boundary-layer rake; the other sensor devices are in the immediate vicinity of the rake.

Three-dimensional coordinates of the forward fuselage for the A5A airplane were not available for this paper; however, normalized coordinates which approximate the contour of the lower-surface centerline are shown in table 1 for the region from the theoretical nose apex to the boundary-layer complex. A deviation from the desired clean contour of an ogive type of fuselage nose was caused by the airspeed boom and its accompanying protuberances. The boom extended forward from what would otherwise have been the nose apex (figs. 1 to 3). The probable effect of this would be to (1) cause a turbulent boundary layer over the entire length of the nose from the effects of either the added upstream surface or the protuberance-induced vortices; and (2) cause some thickening of the boundary layer at the test panel beyond that which would exist without the boom for a given angle of attack.

A closeup view of the test panel is shown in figure 4. The surface of the panel was painted metal, which was sanded smooth. The nose surface ahead of the test panel was smooth fiber glass, and the joint between the fiber glass and the test panel was a close fit which did not cause a discontinuity in the contour of the lower-fuselage surface.

In-flight pressure-distribution data for the bottom centerline of the A5A airplane are not available, and efforts to obtain wind-tunnel data taken during the development of the airplane were unsuccessful. However, wind-tunnel data from models of two other aircraft were examined. Typical examples of these data from the bottom centerlines of an F-111 model (unpublished) and from a model of the X-15 airplane (ref. 17) are shown in figure 5. The data suggest that the pressure gradient of the A5A bottom centerline was probably slightly adverse through the region corresponding to the boundary-layer-complex station of the present study. For one model, increase in angle of attack made the gradient somewhat more adverse; thus angle of attack may have had a similar effect on the A5A airplane. The maximum gradient suggested by

these model data is very slight, however, inasmuch as the computed pressure gradient parameter $\frac{\delta^*}{\tau}\frac{dp}{d\ell}$ would never be greater than 0.3.

The demonstration airplane was flown to provide quasi-steady-state conditions over a local Mach number range from 0.51 to 1.72. Because the test conditions encompassed a combination of altitudes and velocities, data were obtained over a range of angle of attack from about 0° to 7°.

INSTRUMENTATION

External Sensors

The primary sensors for this study are the boundary-layer rake and the flush static orifice (fig. 4). For the Mach number range of this study, these sensors and a knowledge of free-stream stagnation temperature can provide the conventional boundary-layer profiles in terms of Mach number or velocity ratio as a function of distance from the surface. Because the pressure recorder had limited capacity, only seven channels could be assigned to the boundary-layer rake. Thus, the profiles presented are represented by fewer impact-pressure probes than would ordinarily be desirable for a boundary-layer experiment.

Also shown in figure 4 is a surface impact probe which provided a means of calculating local skin friction. Two other devices were included within this boundary-layer complex for the purpose of assessing their flight worthiness. These were a commercially available skin-friction balance, which was later successfully demonstrated on the X-15 airplane (ref. 9), and a traversing pitot-probe mechanism intended to replace conventional boundary-layer rakes for some future boundary-layer studies. The flush static orifice, the center of the friction gage, and the openings of all impact probes were at the same axial fuselage station, with the rake being mounted on the fuselage lower-surface centerline.

The skin-friction balance did not function properly for this study because of dust and lint contamination, and the traversing-probe drive motor was found to be underpowered and did not operate for the tests which imposed the greatest loads on the drive mechanism. Thus, the paper concentrates on the results of what have been referred to as the primary sensors, though some results from the traversing probe are included to provide supplementary edge conditions beyond the reach of the rake, and several "Clauser type" local-friction-coefficient determinations.

Supporting data were used, though not all are presented, in the form of free-stream Mach number, free-stream static pressure, angle of attack, angle of sideslip, and stagnation temperature. Each of these parameters was sensed or derived from locations ahead of the aircraft nose, since the sensors were supported by or contained in the nose boom. The angle-of-attack values used are indicated values which include upwash effects estimated to be a maximum of 5 percent of true angle of attack.

Recording

All data were recorded within the airplane. The pressure data for the boundary-layer complex were recorded on a standard NACA 12-cell flight photo-recording manometer. Free-stream stagnation temperature and the available traversing-probe position values were recorded on an oscillograph. All other parameters pertinent to the demonstration were recorded by standard flight recorders, and all data were synchronized by a common timer.

DATA-REDUCTION PROCEDURES

The boundary-layer impact-pressure data were transformed to velocity-profile form by assuming that the static pressure as measured on the test-panel surface was constant through the boundary layer and that the stagnation temperature was constant through the boundary layer and equal to the value measured ahead of the aircraft nose.

Wall-temperature values were not available for these tests; consequently, the analysis was made by assuming that wall conditions were adiabatic. This should be an acceptable assumption because the data runs that were 2 minutes in duration showed no effects that could be attributed to varying wall temperature. Furthermore, the data runs were preceded by stabilized flight at the same conditions for 1 to 5 minutes.

The equations and tables of reference 18 were used to compute local Mach number. The boundary-layer velocities were calculated by using the following expression:

$$u = 49.02M \left[\frac{T_s}{1 + \frac{(\gamma - 1)}{2} M^2} \right]^{1/2}$$

Because the choice of boundary-layer-edge conditions is somewhat arbitrary, the possible effect on θ of varying the definition of δ is evaluated later. The lower values of δ used were derived from the distance y, corresponding to 0.99 of the maximum measured u. The higher values used were determined at the distances which corresponded approximately to the maximum measured u. This was done because the value of δ according to Coles in reference 6 (in which a plot of y versus $\left(1 - \frac{u}{u_{max}}\right)^{2/3}$ is used) tends to be closer to u_{max}.

In three instances, the traversing probe was needed to define the boundary-layer-edge conditions, and for several other profiles it verified that the outer probe of the rake had indeed attained edge conditions.

Because the boundary-layer thickness δ was small, between 2 and 4 percent, compared with the local surface radius of curvature, momentum thickness θ and displacement thickness δ^* were calculated by using the following flat-plate relationships:

$$\theta = \int_0^{\delta} \frac{\rho u}{\rho_1 u_1} \left(1 - \frac{u}{u_1}\right) dy$$

$$\delta^* = \int_0^{\delta} \left(1 - \frac{\rho u}{\rho_1 u_1}\right) dy$$

When parameters are presented for fluid properties based on a reference temperature, the T' method of Sommer and Short is used (refs. 19 and 20).

Local skin-friction coefficients were derived from the flight data by two methods. The surface impact, or Preston, probe method was applied by using the calibrations for compressibility effects from reference 10. The other method was a Clauser type of determination (ref. 12) which required a transformation procedure to account for compressibility effects, such as that developed by Baronti-Libby (ref. 21). However, the transformation for the Clauser determination used is from Allen or Allen and Tudor (refs. 22 and 23) because of its relative ease of application. This adaptation of the Clauser determination is based on the Fenter-Stalmach version of the wall law for compressible flow (ref. 24).[3]

Although both the Preston probe calibration of reference 10 and the Clauser charts of reference 23 represent flat-plate boundary layers, they were applied without modification to the data of the present demonstration because of the aforementioned small ratio of boundary-layer thickness to local surface radius of curvature. It is realized that other factors such as changing angle of attack or the upstream flow history might be considered as undesirable deviations from the more ideal conditions from which these two methods were derived. Nevertheless, in view of the significant distance of the boundary-layer complex from the rapid changes in surface geometry and the relatively low pressure gradient which is believed to exist, these techniques were applied to the profiles of the study.

ACCURACY

An estimate was made of the effect of errors in measuring pressures on the values of skin friction calculated from these pressures. Experience at the Flight Research Center with the NACA type of pressure recorder has yielded errors in measuring local pressures of about 1 percent for impact pressure and 2 percent for static pressure. This results in a possible local Mach number error of ± 0.02 for the present study when the signs of these two errors are opposite, which is the most adverse arrangement.

The effects of errors on the Clauser type of calculation were analyzed on the assumption that the errors for the subject boundary-layer complex were similar to those noted in the preceding paragraph. The results showed errors of ± 5 percent in C_f at the lower Reynolds numbers and subsonic speeds to about ± 3 percent at high Reynolds numbers and supersonic speeds. In addition to errors caused by the pressure measurements, there was an added uncertainty in deriving C_{f_i} because of possible inadequacies in the compressibility transformations and the constants in the basic

[3]The charts of reference 23 were used as a sensor would be, without concern for the inner workings of the sensor; i.e., without concern that the constants in the incompressible wall law used by Fenter and Stalmach represent Cole's 1953 values or that the Fenter and Stalmach treatment of compressibility effects is based on a different temperature function than the T' function of Sommer and Short.

equation for incompressible flow (used in the charts of ref. 23). A presentation of transformed C_f and R_θ, such as occurs later in this paper, will also be affected by errors in the momentum thickness Reynolds number. It is estimated that these other error sources added to the error from pressure uncertainties would increase the net uncertainty in an incompressible C_f versus R_θ presentation to maximum values within ±10 percent for the Clauser type of calculation. The scatter of the calculated values about a mean line fairing which could be drawn through the data of this type of presentation and the level of that mean line will be seen to be consistent with this estimate, assuming in this instance that a comparison to the Kármán-Schoenherr curve should be considered as a criterion.

The extent to which the Clauser- and Preston-determined friction coefficients are affected by deviations of the test panel from a flat plate is not known. These techniques were applied, however, because, as stated previously, the boundary-layer thickness is small (from 2 percent to 4 percent) compared with the local surface radius of curvature at the test station.

Because the Preston probe results for this demonstration rely on an additional pressure measurement, the error can be larger. It is believed that the maximum error for a Preston probe at the lower centerline of the A5A airplane could have reached ±13 percent (in terms of a presentation of transformed C_f versus transformed R_θ). The Preston probe was displaced from the centerline of the airplane, however, and it is believed that lateral flow may have imposed additional effects on these results at angles of attack above 2°. The reason for the possible lateral flow is discussed later.

The various computed thickness parameters are subject to the definition of δ. The boundary-layer thickness δ is a rather arbitrary quantity, as was mentioned in the preceding section. Thus, two definitions of δ were considered, and the effects of these on θ are shown later. The difference in θ calculated for the two different edge conditions can be considerable; however, the interpretation of data involving θ is not affected in a qualitative sense.

PRESENTATION OF THE BOUNDARY-LAYER PROFILES

Time-averaged data from 13 boundary-layer profiles are presented. The data were obtained during flight at nearly constant Mach number and altitude; thus, short-period dynamic effects were eliminated. Two examples of these profiles, representing the extremes in angle of attack, are presented in figure 6 in terms of velocity ratio as a function of distance from the skin and in terms of the wall and defect law. Data for all the profiles are presented in table 2.

DISCUSSION

The Boundary Layer

Boundary-layer-thickness ratios in terms of $\frac{\delta}{x}$ are plotted in figure 7 as a

function of R_x.[4] The flight data, representing local boundary-layer-edge Mach numbers from 0.51 to 1.72, are compared with three estimates of the variation of $\frac{\delta}{x}$ with R_x for flat-plate turbulent incompressible flow. These predictions of $\frac{\delta}{x}$ bear little resemblance to the array of the flight data, but, of course, the flight data contain angle-of-attack, three-dimensional, and compressible effects. Before these effects are treated, the data will be presented as $\frac{\theta}{x}$ (fig. 8), inasmuch as θ is believed to be more reliably defined than δ.[5]

In figure 8, the flight data are compared with curves for incompressible flow derived from the expressions attributable to Hoerner and Granville in figure 7. These curves are applicable over a wider range of Reynolds numbers than the much-used expression

$$\frac{\delta}{x} = \frac{0.37}{R_x^{0.2}}$$

The relationship shown in figure 8, as would be expected, also shows considerable variation of the flight data above and below the incompressible flat-plate predictions. Figure 9 was prepared in an effort to remove the effects of compressibility from the flight data so that the reasons for these variations might be isolated. In figure 9(a) the prediction curves are the same incompressible expressions shown in figure 8, and the flight data have been adjusted to incompressible conditions through the flat-plate transformation coefficients indicated. These coefficients provide density and viscosity reference conditions based on the reference temperature T' for an adiabatic wall (ref. 19).

If attention is given to the grouping of the flight data with respect to angle of attack in figure 9(a), an interesting pattern appears. The high angle-of-attack data, 6° to 7°, are closer to the curve for slender cones than to the flat-plate predictions. This is consistent in a qualitative sense with results in reference 15 for $\frac{\theta}{x}$ values obtained on curved forebodies which are expanding in cross-sectional-area development; in reference 15, all data such as these are between the flat-plate and slender-cone theoretical curves.

The lowest angle-of-attack data in figure 9(a), 0.1° to 1.0°, are far above the theoretical curves for a flat plate, whereas the intermediate angle-of-attack data (unflagged symbols) are closer to the flat-plate curves. These groupings of the data with respect to angle of attack suggest that the growth of momentum thickness should be examined with angle of attack as the independent variable.

Although the grouping of high and moderate angle-of-attack data would probably be expected, in light of reference 15 and other body-of-revolution results, the low angle-of-attack data are farther above flat-plate theory than other studies would have

[4]Boundary-layer thickness δ as used in this instance and in preparing table 3 is defined as the value of y corresponding to the maximum measured value of u. The effect of such an arbitrary definition is shown in subsequent figures.

[5]These values of θ are presented in table 3 along with other parameters computed from the boundary-layer measurements.

predicted for a simple pointed body. This might be caused by the superimposed boundary layer from the nose boom. The square symbols in figure 9(a) show the transformed ratio of $\frac{\theta}{x}$ when it is assumed that the entire nose-boom boundary layer is superimposed, without thinning of the layer associated with the growing cross-sectional area of the airplane nose.

Significant effects from the nose boom are considered probable only at the lower angles of attack, because at higher angles of attack some of the flow having a history over the boom would tend to be diverted away from the bottom centerline region. In view of this, and because of the previously mentioned thinning effects, the most meaningful values of transformed $\frac{\theta}{x}$ for low angle of attack would probably be between the horizontally flagged circles and squares. This suggests that the gross effect of the nose boom may be significantly greater than superimposition of a boundary layer from a smooth nose boom would cause and that the protuberances on the boom shown in figure 3 may be important.

In the DATA-REDUCTION PROCEDURES section, it was pointed out that two definitions of δ were considered. The effects of these two definitions are presented in figure 9(b) which is in the same format as figure 9(a). The figure shows that, though the levels of $\frac{\theta}{x}$ are systematically affected by the choice of δ, the results are qualitatively unchanged; that is, there is evidence of both an angle-of-attack influence and, it is believed, significant nose-boom and protuberance effects.

To evaluate more explicitly the influence of angle of attack and nose-boom protuberance effects, figure 10 was prepared. The ordinate consists of $\overline{\theta}$ (θ for curved surface) transformed to $M = 0$ and divided by $\overline{\theta}$ (θ for flat plate) for the corresponding Reynolds number. When these ratios are plotted as a function of angle of attack, a consistent trend is apparent. These flight data are shown, as previously, for a range of edge conditions and at low angle of attack for two assumed origins of turbulence ($x = 200$ in. (508 cm) and 290 in. (736 cm)). Again, the precise choice of edge conditions is not critical in demonstrating an angle-of-attack influence. In addition, because of the expected boundary layer thinning effects, it is believed that the real relationship of $\left(\frac{\overline{\theta}}{\overline{\theta}_t}\right)_i$ for flight would be closer to the circles than to the squares for low angle of attack.

Included for comparison in figure 10 is the curve based on a method used by Allen and Monta (ref. 15) which approximates the influence of the fuselage lower centerline contour back to the location of the boundary-layer complex, and also approximates the angle-of-attack effects. In this instance, liberties were taken with the method to permit the angle-of-attack changes to be considered as deformations of the body cross-sectional-area development. Thus, the fuselage lower centerline contour relative to the free-stream flow is properly accounted for in the prediction at any angle of attack, but the local body radius is not properly simulated. For this curve the numerator of the ordinate parameter is $\overline{\theta}$ calculated by using reference 15, modified for angle of attack. The denominator is $\overline{\theta}$ at zero angle of attack, derived from reference 1 through the relationship of C_F to θ given in the SYMBOLS section. Comparison of

the flight-derived data with the prediction suggests, as might be expected, that as angle of attack increases above some critical level the effects of the nose boom and its protuberances are reduced or almost eliminated by being diverted away from the bottom centerline.

The apparent significant effect of the nose boom on θ (other thickness parameters are also affected) suggests that designers should be cautious about such protuberances. Hardware of this type is commonly used on operational aircraft, though the wind-tunnel models of the airplane do not ordinarily include such detail. Thus, the thickness of the boundary layer on parts of the full-scale aircraft may be significantly greater than would have been predicted, and, more important, the subsequent effects of increased displacement thickness on the surface pressures may cause the separation characteristics over the downstream parts of an operational airplane to be more adverse than demonstrated by the model.

Because θ obtained from the present demonstration is influenced by angle of attack, it is appropriate to determine whether the boundary-layer-shape factor H $\left(H = \frac{\delta^*}{\theta}\right)$ is affected by angle of attack. The flight values of H are first compared to a predicted variation of shape factor with Mach number in figure 11(a). The predicted values are derived from the following expression (from ref. 28) which assumes a power law:

$$H = \frac{n + 2}{n}\left(1 + 0.344\, M_1^2\right)$$

where

$$\frac{(n + 2)}{n} = H_i \quad \text{(ref. 25 or 26)}$$

Because this expression presents H as a function of the profile index, the profile indices of the several flight profiles are shown in figure 11(b). These flight values of n are shown as a function of transformed Reynolds number and are compared with wind-tunnel results from reference 28, also plotted with transformed Reynolds numbers, and a curve derived from early incompressible pipe-flow data in reference 2. The variations of the indices n from flight are in general agreement with the wind-tunnel results and the pipe-flow values. These indices for the profiles obtained in flight, as derived from log plots such as those in figure 6, varied from slightly greater than 7 to almost 11. The flight values of H (fig. 11(a)) are significantly higher than the calculated curves for corresponding values of n. The level of the individual flight values of H considered with regard to the angle-of-attack values, rounded to the nearest degree, suggests that angle of attack may influence shape factor.

The influence of angle of attack is more evident in figure 12 than in figure 11(a). The flight values of H are plotted as a function of M_1^2 because some experiments, including those of reference 28, demonstrate such a relationship. The angle-of-attack values are indicated in the same manner as in figure 11(a). Two straight lines were added to this presentation which seem to demonstrate, at least approximately, an M^2 relationship, and tend to emphasize the grouping of data for specific angle-of-attack values in a rather orderly manner. Extrapolation of the line for $\alpha \approx 0°$ to $M = 0$ results in an incompressible approximation of the flight shape factor of about 1.34.

A more meaningful way to evaluate the influence of angle of attack would be to normalize the data through a denominator which accounts for the Mach number and Reynolds number of the flight data. This has been done in figure 13(a) in which the following expression from reference 28 is used:

$$H_i = \frac{H}{\left(1 + 0.344\ M_1^2\right)}$$

The following expression which was used by Nash and Macdonald (ref. 29) and in references 30 and 31 is also used in figure 13(b):

$$H_i = \left[\frac{(H + 1)}{1 + 0.178\ M_1^2}\right] - 1$$

These equations were used to reduce the flight values to incompressible conditions (the numerators of the ordinates). The denominators of the ordinates were obtained from the proposed law of Smith and Walker (ref. 4). In figures 13(a) and 13(b), the denominator of the ordinate is chosen for the transformed Reynolds number $R_\theta \frac{\mu_1}{\mu'}$ of the corresponding flight-derived numerator; in addition, the denominators represent two-dimensional flow with zero longitudinal pressure gradient.

Figure 13(a) indicates that accounting for compressibility by Fenter's expression segregates the subsonic and supersonic values of H, and, at subsonic speeds, angle of attack appears to be an influential factor. The relationship from Nash (fig. 13(b)) also shows that angle of attack exerts an orderly influence for the subsonic results, and the differences in level attributable to speed regime are not significant. The flight-shape factors extrapolate to values from about 4 percent to 9 percent above the flat-plate incompressible values for zero longitudinal pressure gradient and zero angle of attack, depending on the choice of method for accounting for compressibility. The proposed law of Coles (ref. 32) or the use of $\frac{n + 2}{n}$ for $\overline{H}_i$ would have resulted in similar trends of $\left(\frac{H_f}{\overline{H}}\right)_i$ with α.

Because the flight values of H are higher than any of the expressions for flat-plate zero-pressure-gradient flow, the presence of a somewhat adverse pressure gradient is suspected, as suggested by references 12, 25, or 33. Although pressure-distribution data from the bottom centerline of the A5A airplane are not available, it was shown in figure 5 and in the TEST FACILITY AND CONDITIONS section that the lower centerline location was likely to experience a mild adverse gradient which may increase with angle of attack.

Local Friction Coefficient

Numerous investigators have shown that the local skin friction for flow conditions which are not strongly accelerated or close to separation is a function of a thickness Reynolds number R_θ and a boundary-layer-shape parameter such as H (refs. 29,

and 33 to 35, for example). Reference 36 indicates that when a pressure gradient is accompanied by converging or diverging flow, as over a pointed or waisted body, the relationship of friction to pressure gradient or shape factor is more complex. Furthermore, references 36 to 38 show that the upstream history of the flow can further complicate the relationship of friction, Reynolds number, and shape parameter.

Although flow convergence or divergence effects should have been negligible at the location of the boundary-layer complex, the relationship of C_f, R_θ, and H would seem to be subject to a relatively distant varying upstream history. These upstream changes could result from the varying influence of α on the superimposed nose boom and nose-boom-protuberance effects and by the divergence of the flow as it moved over the expanding portion of the fuselage nose.

The present boundary-layer experience is not comprehensive enough to provide a definitive relationship between the upstream history, the profile shape, and local skin friction. An observation can be made, however, of the friction levels which were obtained in the presence of the aforementioned changing upstream history. Local friction coefficients were derived from the flight data by two methods: the surface impact probe (Preston) technique, and a Clauser type of determination. The DATA-REDUCTION PROCEDURES section describes the means by which the Clauser and Preston techniques were adapted for use in compressible flow.

The relationship of local friction coefficients obtained by these methods is shown in figure 14. The Clauser method was applied both to the profiles obtained from the traversing probe and to the less comprehensive profiles obtained from the boundary-layer rake. The Clauser-determined values of friction in figure 14(a) agree well with one another and indicate a level of friction coefficient which is close to the incompressible curve of Kármán-Schoenherr. Such relatively consistent values are of interest for the Clauser approach when it is recalled that: (1) the transformed shape factors are somewhat higher than flat-plate values for no pressure gradient; (2) there is evidence from two airplane models that the lower centerline should have a mild adverse pressure gradient, which may increase with angle of attack; and (3) the upstream history of each profile is probably different.

The transformed friction-coefficient values obtained from the surface impact probe are not as consistent as the Clauser-determined values. This does not necessarily imply less reliability for this method per se, but may be a systematic grouping inherent in the present application of the Preston probe. There is a tendency, for example, for the friction values which lie significantly below the Kármán-Schoenherr curve to represent the higher angles of attack or ratios of $\left(\frac{H_f}{\overline{H}}\right)_i$, and, conversely, the remaining friction values derived from the Preston probe to represent the lower values of angle of attack and $\left(\frac{H_f}{\overline{H}}\right)_i$.

It is suggested that this segregation of data for the surface impact probe may not be related to the changes in shape factor, as in references 29 or 33 to 35, but may pertain to the local portion of the wall-law region which is being surveyed and the relative values of the body crossflow velocity. The surface impact probe for this installation

experienced flow for $\frac{u}{u_1}$ values near or below 0.6; whereas, the Clauser determination was made at ratios of 0.7 and greater. Reference 12 emphasizes that, with an adverse pressure gradient, a boundary layer can experience lateral flow in the lower energy regions if even small three-dimensional conditions are imposed on the flow, an observation certainly consistent with airfoil experience. Thus, it may be that the surface impact probe which was mounted slightly off the fuselage centerline and in the lower velocity region of the boundary layer was experiencing lateral flow which caused the calculated local friction to appear lower at angles of attack greater than 2°.

Figure 14(b) compares the local friction coefficients of the present study, as obtained from the Clauser determination, with flight results from reference 39. The data from reference 39 have been interpreted through the Clauser technique from profile data for the upper surface of the wing of a Mirage IV airplane. These data were transformed to incompressible fluid properties from flight Mach numbers between 1.77 and 2.14. The results of the present study and reference 39 seem to be compatible.

The Clauser-derived local friction coefficients of the present study are shown again in figure 15 as a function of transformed R_x. The method of presentation is somewhat similar to that of figure 9 in which an effort was made to identify the low, moderate, and high angles of attack which the data represent. The local friction coefficients of figure 15 and the $\frac{\theta}{x}$ results of figure 9 are shown to be qualitatively compatible; the high angle-of-attack data tend to be grouped close to the slender-cone curve and the low angle-of-attack data tend to be close to or lower than the flat-plate C_f predictions. To appreciate this compatibility the reader must be aware of the inverse relationship of flat-plate and slender-cone values of C_f and $\frac{\theta}{x}$ when presented as a function of R_x (as can be observed in ref. 15).

CONCLUDING REMARKS

A flight demonstration of a pressure-sensing complex for defining boundary-layer characteristics defined some parameters which merited comparison with predictions. These comparisons indicated the following results:

Local transformed friction coefficients obtained from a Clauser-type of determination were close to the incompressible values of Kármán-Schoenherr when presented as a function of momentum thickness Reynolds number. These values were relatively consistent, even though the transformed shape factor H was influenced by angle of attack and the upstream history of the flow was probably different for each of the profiles studied. These transformed local friction coefficients also agreed well with coefficients derived from profiles obtained from the wing of the French Mirage IV. The local transformed coefficients of the present study when presented as a function of Reynolds number based on the length of turbulent flow R_x varied above and below the Kármán-Schoenherr curve as angle of attack varied.

In a related manner, turbulent momentum thickness values were significantly influenced by angle of attack. The flight values of momentum thickness for angles of

attack near 6° to 7° were lower than flat-plate values, approaching the levels for slender cones. At angles of attack near 0° to 1°, the momentum thickness θ from flight was higher than flat-plate values. The aircraft nose boom and the protuberances on the boom are believed to be major reasons for the additional thickness at low angles of attack.

Boundary-layer-profile indices varied from slightly greater than 7 to 11, and the variation with Reynolds number was in general agreement with pipe-flow values and two-dimensional wind-tunnel results.

The flight values of shape factor H, adjusted to a Mach number of zero, were higher than flat-plate values. This difference was increased by increasing angle of attack.

Flight Research Center,
National Aeronautics and Space Administration,
Edwards, Calif., February 27, 1970.

REFERENCES

1. Locke, F. W. S., Jr.: Recommended Definition of Turbulent Friction in Incompressible Fluids. DR Rep. No. 1415, Navy Dept., Bur. of Aeronautics, Res. Div., June 1952.

2. Prandtl, L.; and Tietjens, O. G.: Applied Hydro- and Aeromechanics. Dover Publications, Inc., 1957.

3. Dhawan, Satish: Direct Measurements of Skin Friction. NACA Rep. 1121, 1953. (Supersedes NACA TN 2567.)

4. Smith, Donald W.; and Walker, John H.: Skin-Friction Measurements in Incompressible Flow. NASA TR R-26, 1959. (Supersedes NACA TN 4231.)

5. Korkegi, Robert H.: Transition Studies and Skin-Friction Measurements on an Insulated Flat Plate at a Mach Number of 5.8. J. Aeron. Sci., vol. 23, no. 2, Feb. 1956, pp. 97-107, 192.

6. Coles, Donald: Measurements in the Boundary Layer on a Smooth Flat Plate in Supersonic Flow. Jet Prop. Lab., Calif. Inst. Technol.
   I. The Problem of the Turbulent Boundary Layer. Rep. No. 20-69, June 1, 1953.
   II. Instrumentation and Experimental Techniques at the Jet Propulsion Laboratory. Rep. No. 20-70, June 1, 1953.
   III. Measurements in a Flat-plate Boundary Layer at the Jet Propulsion Laboratory. Rep. No. 20-71, June 1, 1953.

7. McDill, Paul Laurence: The Design and Experimental Evaluation of a Skin Friction Balance for Measuring Local Turbulent Shear Stress in the Presence of Heat Transfer at a Mach Number of 5. DRL-453, Univ. of Texas, Jan. 1961.

8. Lyons, Willis Carson, Jr.: The Design of an Acceleration Insensitive Skin Friction Balance for Use in Free Flight Vehicles at Supersonic Speeds. DRL-397, Univ. of Texas, June 1957.

9. Garringer, Darwin J.; and Saltzman, Edwin J.: Flight Demonstration of a Skin-Friction Gage to a Local Mach Number of 4.9. NASA TN D-3830, 1967.

10. Hopkins, Edward J.; and Keener, Earl R.: Study of Surface Pitots for Measuring Turbulent Skin Friction at Supersonic Mach Numbers - Adiabatic Wall. NASA TN D-3478, 1966.

11. Preston, J. H.: The Determination of Turbulent Skin Friction by Means of Pitot Tubes. No. 15,758, British A.R.C., March 31, 1953.

12. Clauser, Francis H.: Turbulent Boundary Layers in Adverse Pressure Gradients. J. Aeron. Sci., vol. 21, no. 2, 1954, pp. 91-108.

13. Wilson, R. E.: Characteristics of Turbulent Boundary Layer Flow Over a Smooth, Thermally Insulated Flat Plate at Supersonic Speeds. DRL-301, Univ. of Texas, June 1, 1952.

14. Matting, Fred W.; Chapman, Dean R.; Nyholm, Jack R.; and Thomas, Andrew G.: Turbulent Skin Friction at High Mach Numbers and Reynolds Numbers in Air and Helium. NASA TR R-82, 1961.

15. Allen, Jerry M.; and Monta, William J.: Turbulent-Boundary-Layer Characteristics of Pointed Slender Bodies of Revolution at Supersonic Speeds. NASA TN D-4193, 1967.

16. Hughes, Donald L.; Powers, Bruce G.; and Dana, William H.: Flight Evaluation of Some Effects of the Present Air Traffic Control System on Operation of a Simulated Supersonic Transport. NASA TN D-2219, 1964.

17. Osborne, Robert S.; and Stafford, Virginia C.: Basic Pressure Measurements on a 0.0667-Scale Model of the North American X-15 Research Airplane at Transonic Speeds. NASA TM X-344, 1960.

18. Ames Research Staff: Equations, Tables, and Charts for Compressible Flow. NACA Rep. 1135, 1953. (Supersedes NACA TN 1428.)

19. Sommer, Simon C.; and Short, Barbara J.: Free-Flight Measurements of Turbulent-Boundary-Layer Skin Friction in the Presence of Severe Aerodynamic Heating at Mach Numbers From 2.8 to 7.0. NACA TN 3391, 1955.

20. Peterson, John B., Jr.: A Comparison of Experimental and Theoretical Results for the Compressible Turbulent-Boundary-Layer Skin Friction With Zero Pressure Gradient. NASA TN D-1795, 1963.

21. Baronti, Paolo O.; and Libby, Paul A.: Velocity Profiles in Turbulent Compressible Boundary Layers. AIAA J., vol. 4, no. 2, Feb. 1966, pp. 193-202.

22. Allen, Jerry M.: Use of Baronti-Libby Transformation and Preston Tube Calibrations To Determine Skin Friction From Turbulent Velocity Profiles. NASA TN D-4853, 1968.

23. Allen, Jerry M.; and Tudor, Dorothy H.: Charts for the Interpolation of Local Skin Friction From Experimental Turbulent Velocity Profiles. NASA SP-3048, 1969.

24. Fenter, Felix W.; and Stalmach, Charles J., Jr.: The Measurement of Local Turbulent Skin Friction at Supersonic Speeds by Means of Surface Impact Pressure Probes. DRL 392, Univ. of Texas, Oct. 21, 1957.

25. Schlichting, Hermann: Boundary-Layer Theory, Sixth Edition. McGraw-Hill Book Co., Inc., 1968, p. 599.

26. Hoerner, Sighard F.: Fluid-Dynamic Drag. Publ. by the author (148 Busteed Dr., Midland Park, N. J.), 1965, pp. 2-3 to 2-5.

27. Granville, Paul S.: The Determination of the Local Skin Friction and the Thickness of Turbulent Boundary Layers From the Velocity Similarity Laws. Rep. 340, David Taylor Model Basin, Oct. 1959.

28. Fenter, Felix W.: A New Analytical Method for the Prediction of Turbulent Boundary Layer Characteristics on a Thermally Insulated Flat Plate at Supersonic Speeds. Rep. No. DRL-343, Univ. of Texas, June 1954.

29. Nash, J. F.; and Macdonald, A. G. J.: A Turbulent Skin-friction Law for Use at Subsonic and Transonic Speeds. C. P. No. 948, British A.R.C., 1967 (Supersedes N. P. L. Aero. Rep. 1206.)

30. Sivells, James C.; and Payne, Robert G.: A Method of Calculating Turbulent-Boundary-Layer Growth at Hypersonic Mach Numbers. AEDC-TR-59-3, (ASTIA No. AD-208774), Arnold Eng. Dev. Center, Mar. 1959.

31. Spence, D. A.: The Growth of Compressible Turbulent Boundary Layers on Isothermal and Adiabatic Walls. Rep. No. Aero 2619, British R.A.E., June 1959.

32. Coles, D. E.: The Turbulent Boundary Layer in a Compressible Fluid. Rep. R-403-PR, The Rand Corp., Sept. 1962.

33. Ludwieg, H.; and Tillmann, W.: Investigations of the Wall-Shearing Stress in Turbulent Boundary Layers. NACA TM 1285, 1950.

34. Nash, J. F.: A Note on Skin-Friction Laws for the Incompressible Turbulent Boundary Layer. NPL Aero Rep. 1135, British A.R.C., Dec. 20, 1964.

35. Rotta, J.: On the Theory of the Turbulent Boundary Layer. NACA TM 1344, 1953.

36. Winter, K. G.: Smith, K. G.; and Rotta, J. C.: Turbulent Boundary-Layer Studies on a Waisted Body of Revolution in Subsonic and Supersonic Flow. Recent Developments in Boundary Layer Research, Pt. II, AGARDograph 97, Mar. 1965, pp. 933-961.

37. Nash, J. F.; and Macdonald, A. G. J.: A Calculation Method for the Incompressible Turbulent Boundary Layer, Including the Effect of Upstream History on the Turbulent Shear Stress. NPL Aero Report 1234, British A.R.C., May 1967.

38. Bradshaw, P.; and Ferriss, D. H.: The Effect of Initial Conditions on the Development of Turbulent Boundary Layers. NPL Aero Report 1223, British A.R.C., Feb. 3, 1967.

39. Erlich, E.: Sondage de la Couche Limite en Vol Supersonique sur L'Avion "Mirage IV." O.N.E.R.A. paper presented at 3e Colloque Aerodynamique de l'A.F.I.T.A.E., Marseille, France, November 8-10, 1966.

TABLE 1.– COORDINATES OF LOWER-FUSELAGE CENTERLINE FROM NOSE APEX TO BOUNDARY-LAYER-RAKE COMPLEX

$\frac{a}{l}$ (6)	$\frac{z}{l}$	$\frac{a}{l}$	$\frac{z}{l}$
0	0	0.2560	0.0531
0.0040	0.0094	.2756	.0547
.0079	.0118	.2953	.0559
.0118	.0134	.3150	.0571
.0197	.0157	.3544	.0594
.0275	.0181	.3938	.0614
.0394	.0212	.4331	.0630
.0591	.0256	.4725	.0646
.0788	.0295	.5119	.0665
.0985	.0331	.5512	.0677
.1181	.0362	.6300	.0687
.1378	.0394	.7088	.0687
.1575	.0421	.7875	.0687
.1772	.0449	.8662	.0687
.1969	.0472	.9450	.0687
.2165	.0496	1.000	.0687
.2363	.0516	------	------

[6] l is the axial distance, 200 inches (508 cm), from the nose apex to the boundary-layer-rake complex fuselage station

TABLE 2.– MEASURED BOUNDARY-LAYER-VELOCITY PROFILES

Profile A
[$M_1 = 0.51$; $\alpha = 7.0°$]

y		$\frac{u}{u_1}$
in.	cm	
0.080	0.203	0.696
.166	.422	.747
.326	.828	.810
.486	1.234	.855
1.209	3.071	.963
2.013	5.113	.990
2.815	7.150	1.000

Profile B
[$M_1 = 0.81$; $\alpha = 2.0°$]

y		$\frac{u}{u_1}$
in.	cm	
0.080	0.203	0.679
.166	.422	.731
.326	.828	.785
.486	1.234	.816
1.209	3.071	.910
2.013	5.113	.970
2.815	7.150	1.000

Profile C
[$M_1 = 0.60$; $\alpha = 6.4°$]

y		$\frac{u}{u_1}$
in.	cm	
0.080	0.203	0.690
.166	.422	.744
.326	.828	.805
.486	1.234	.849
1.209	3.071	.957
2.013	5.113	.990
2.815	7.150	1.000

Profile D
[$M_1 = 0.90$; $\alpha = 3.4°$]

y		$\frac{u}{u_1}$
in.	cm	
0.080	0.203	0.641
.166	.422	.702
.326	.828	.764
.486	1.234	.808
1.209	3.071	.912
2.013	5.113	.982
2.815	7.150	1.000

Profile E
[$M_1 = 0.90$; $\alpha = 4.7°$]

y		$\frac{u}{u_1}$
in.	cm	
0.080	0.203	0.646
.166	.422	.704
.326	.828	.766
.486	1.234	.820
1.209	3.071	.924
2.013	5.113	.987
2.815	7.150	1.000

Profile F
[$M_1 = 1.26$; $\alpha = 3.4°$]

y		$\frac{u}{u_1}$
in.	cm	
0.080	0.203	0.666
.166	.422	.724
.326	.828	.775
.486	1.234	.807
1.209	3.071	.898
2.013	5.113	.973
2.815	7.150	1.000

Profile G
[$M_1 = 1.53$; $\alpha = 2.2°$]

y		$\frac{u}{u_1}$
in.	cm	
0.080	0.203	0.658
.166	.422	.720
.326	.828	.772
.486	1.234	.806
1.209	3.071	.906
2.013	5.113	.968
2.815	7.150	1.000

Profile H
[$M_1 = 1.36$; $\alpha = 2.4°$]

y		$\frac{u}{u_1}$
in.	cm	
0.080	0.203	0.661
.166	.422	.716
.326	.828	.767
.486	1.234	.805
1.209	3.071	.889
2.013	5.113	.965
2.815	7.150	1.000

TABLE 2.– CONCLUDED

Profile I
[$M_1 = 0.82$; $\alpha = 6.2°$]

y		$\frac{u}{u_1}$
in.	cm	
0.080	0.203	0.647
.166	.422	.705
.326	.828	.775
.486	1.234	.840
1.209	3.071	.943
2.013	5.113	.986
2.815	7.150	1.000

Profile J
[$M_1 = 0.64$; $\alpha = 3.8°$]

y		$\frac{u}{u_1}$
in.	cm	
0.080	0.203	0.650
.166	.422	.702
.326	.828	.763
.486	1.234	.816
1.209	3.071	.913
2.013	5.113	.974
2.815	7.150	1.000

Profile K
[$M_1 = 1.72$; $\alpha = 1.0°$]

y		$\frac{u}{u_1}$
in.	cm	
0.080	0.203	0.625
.166	.422	.687
.326	.828	.745
.486	1.234	.780
1.209	3.071	.861
2.013	5.113	.925
2.815	7.150	.971
4.300	10.92	1.000

Profile L
[$M_1 = 0.81$; $\alpha = 0.3°$]

y		$\frac{u}{u_1}$
in.	cm	
0.080	0.203	0.669
.166	.422	.716
.326	.828	.762
.486	1.234	.787
1.209	3.071	.870
2.013	5.113	.926
2.815	7.150	.966
4.300	10.92	1.000

Profile M
[$M_1 = 1.54$; $\alpha \approx 0.1°$]

y		$\frac{u}{u_1}$
in.	cm	
0.080	0.203	0.655
.166	.422	.707
.326	.828	.749
.486	1.234	.774
.807	2.050	.808
1.209	3.071	.849
2.013	5.113	.920
2.815	7.150	.956
3.950	10.03	1.000

TABLE 3.– CALCULATED VALUES OBTAINED FROM MEASURED BOUNDARY-LAYER-VELOCITY PROFILES

Profile	δ^*, in. (cm)	θ, in. (cm)	H	n	u_1, ft/sec (m/sec)	M_1	$\frac{T'}{T_1}$	$\frac{\mu_1}{\mu'}$	$C_{f,pp}$	$C_{f,tp}$	$C_{f,r}$	R_θ	R_x (7)
A	0.244 (0.620)	0.156 (0.396)	1.57	8.50	530 (161.5)	0.51	1.029	0.978	2.13×10^{-3}	2.34×10^{-3}	2.25×10^{-3}	2.42×10^{4}	3.11×10^{7}
B	.353 (.897)	.210 (.533)	1.68	9.20	847 (258.2)	.81	1.072	.948	1.80	1.90	1.95	5.19	4.94
C	.254 (.645)	.157 (.399)	1.62	8.42	604 (184.1)	.60	1.040	.970	2.07	2.35	2.30	2.35	3.00
D	.366 (.930)	.204 (.518)	1.79	7.62	854 (260.3)	.90	1.094	.933	1.70	1.94	1.98	3.21	3.15
E	.346 (.879)	.191 (.485)	1.81	7.57	872 (265.8)	.90	1.094	.933	1.87	2.12	2.13	2.13	2.23
F	.439 (1.115)	.208 (.528)	2.11	9.97	1199 (365.5)	1.26	1.184	.878	2.06	2.00	1.95	3.13	3.01
G	.483 (1.227)	.198 (.503)	2.44	8.47	1443 (439.8)	1.53	1.256	.839	1.98	1.95	1.93	2.70	2.73
H	.505 (1.283)	.228 (.579)	2.22	8.88	1290 (393.2)	1.36	1.212	.863	2.07	----	1.90	3.38	2.95
I	.311 (.790)	.175 (.445)	1.77	7.34	781 (238.0)	.82	1.079	.943	2.06	2.34	2.39	1.35	1.54
J	.336 (.853)	.209 (.531)	1.60	7.93	604 (184.1)	.64	1.047	.965	1.93	2.40	2.20	2.32	2.22
K	.753 (1.913)	.282 (.716)	2.67	8.16	1683 (513.0)	1.72	1.337	.800	1.45	----	1.52	6.03	4.28
L	.507 (1.288)	.313 (.795)	1.62	9.65	889 (271.0)	.81	1.073	.947	1.71	----	1.70	11.61	7.42
M	.735 (1.867)	.306 (.777)	2.40	10.70	1549 (472.1)	1.54	1.271	.832	----	----	1.42	10.64	6.94

[7] Based on x = 200 in. (508 cm).

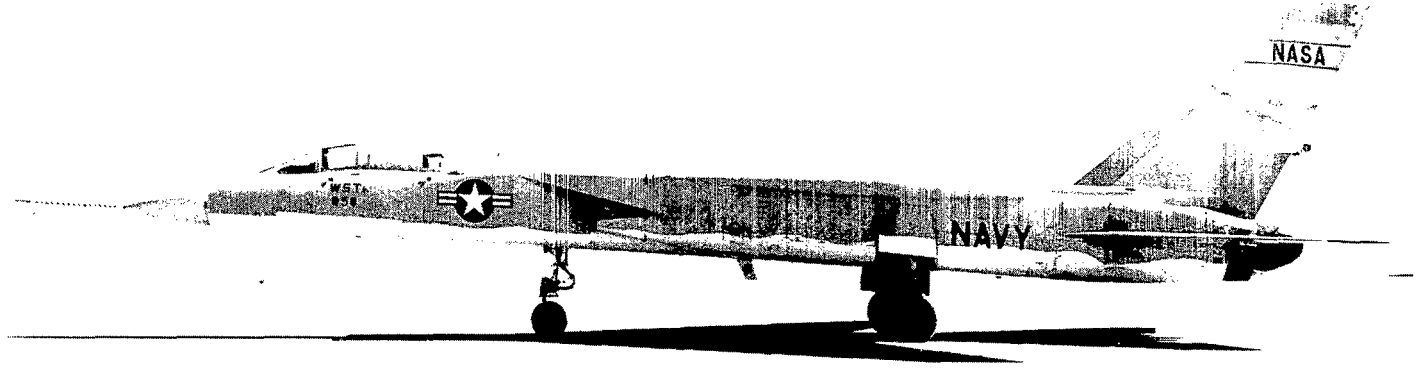

Figure 1. The A5A demonstration airplane. E-10548

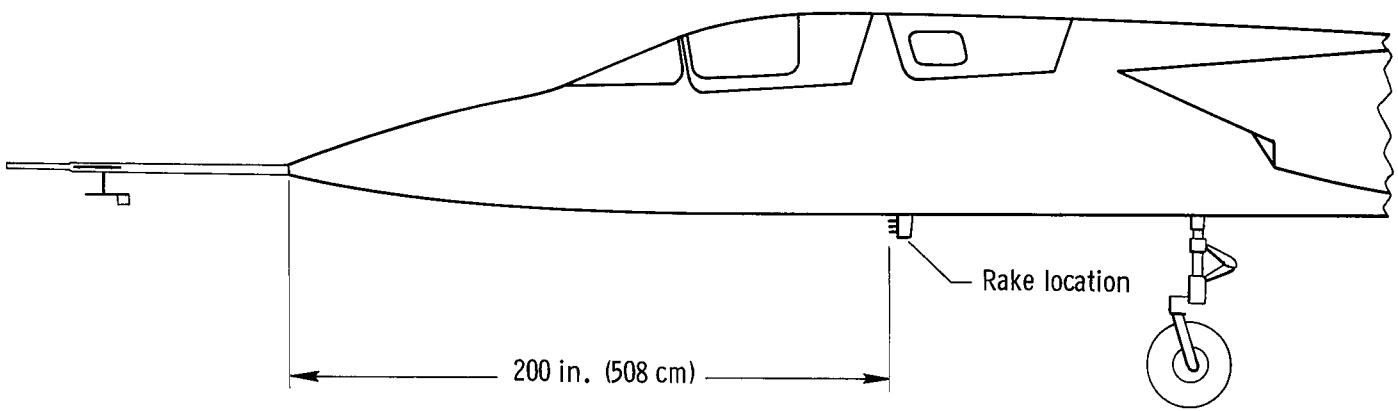

Figure 2. Sketch showing location of boundary-layer rake. (Rake not drawn to scale).

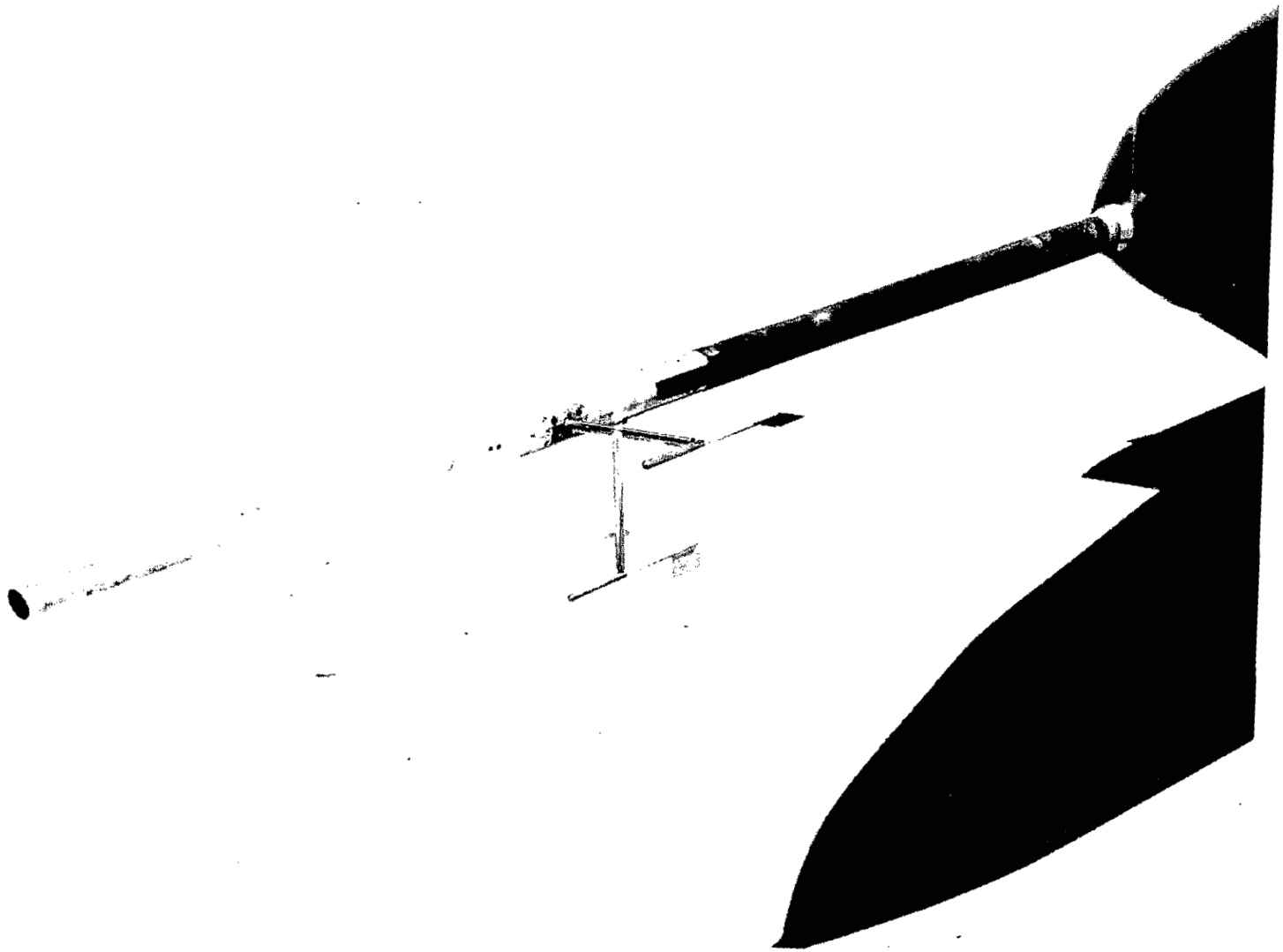

Figure 3. Close-up view of flow-direction shafts similar to those protruding from the A5A nose boom. E-2357

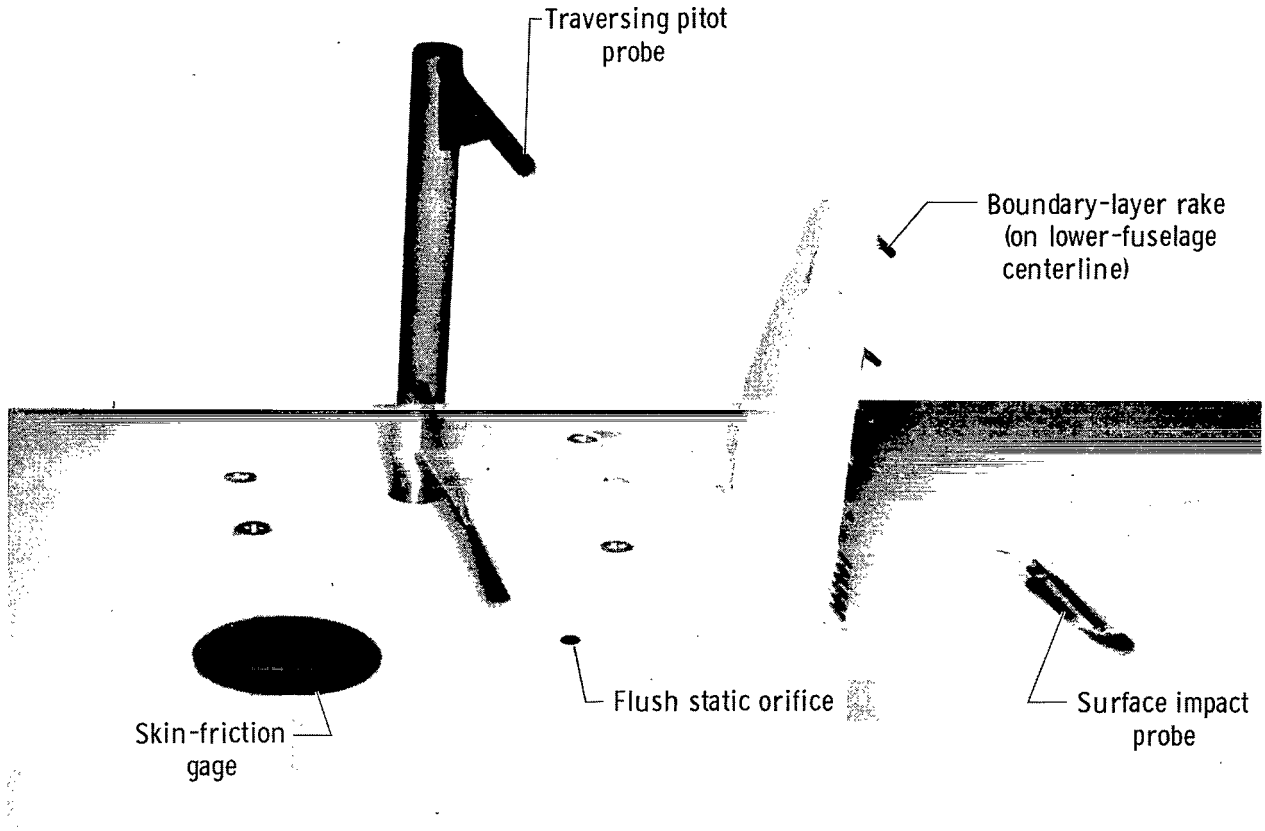

Figure 4. Boundary-layer complex. E-18775

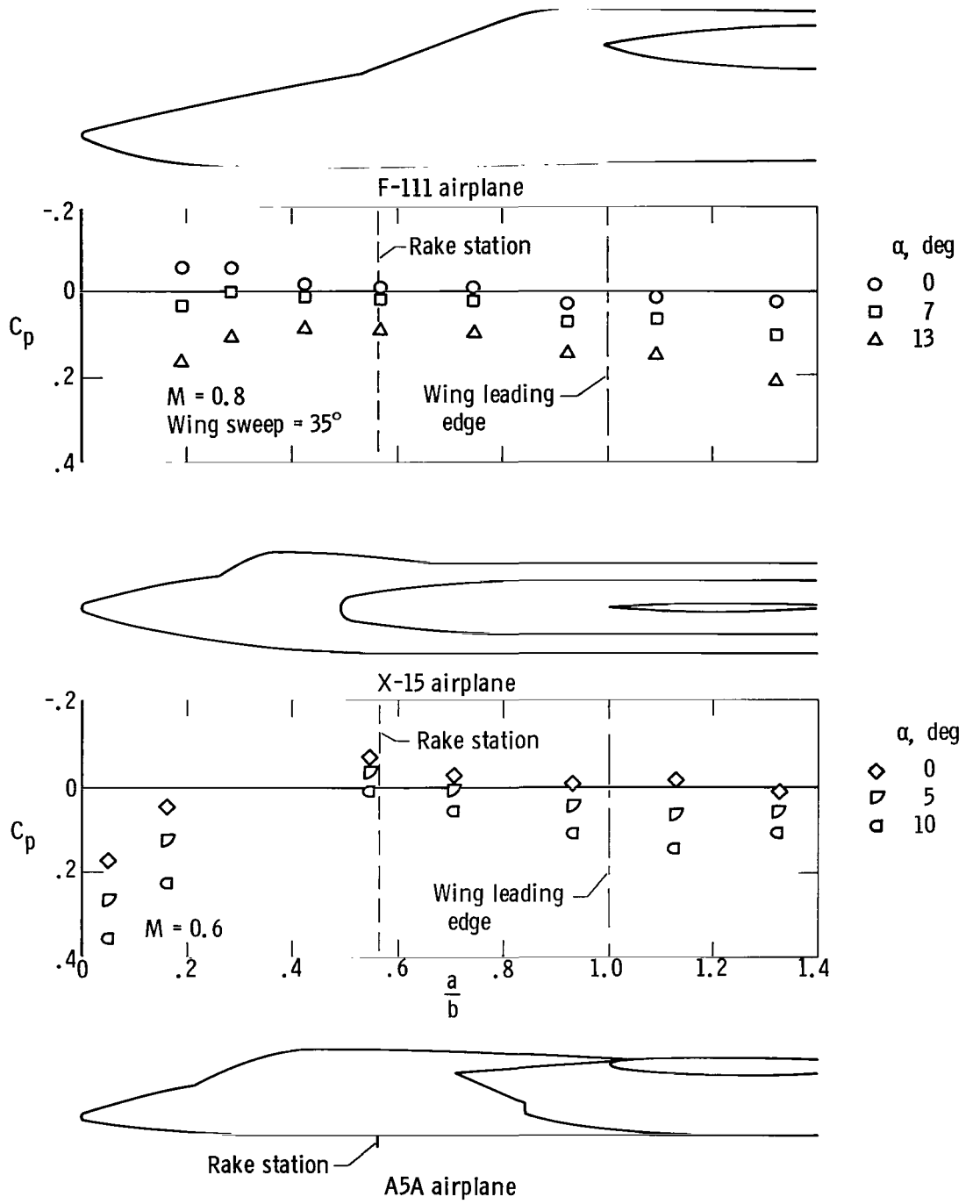

(a) Subsonic.

Figure 5. Pressure coefficients for the bottom centerlines of two airplane model forebodies shown as a function of distance from the nose apex to the wing leading edge for subsonic and supersonic speeds. (Abscissa of plots scaled to correspond with the nose-to-wing-leading-edge distances of forebody sketches.)

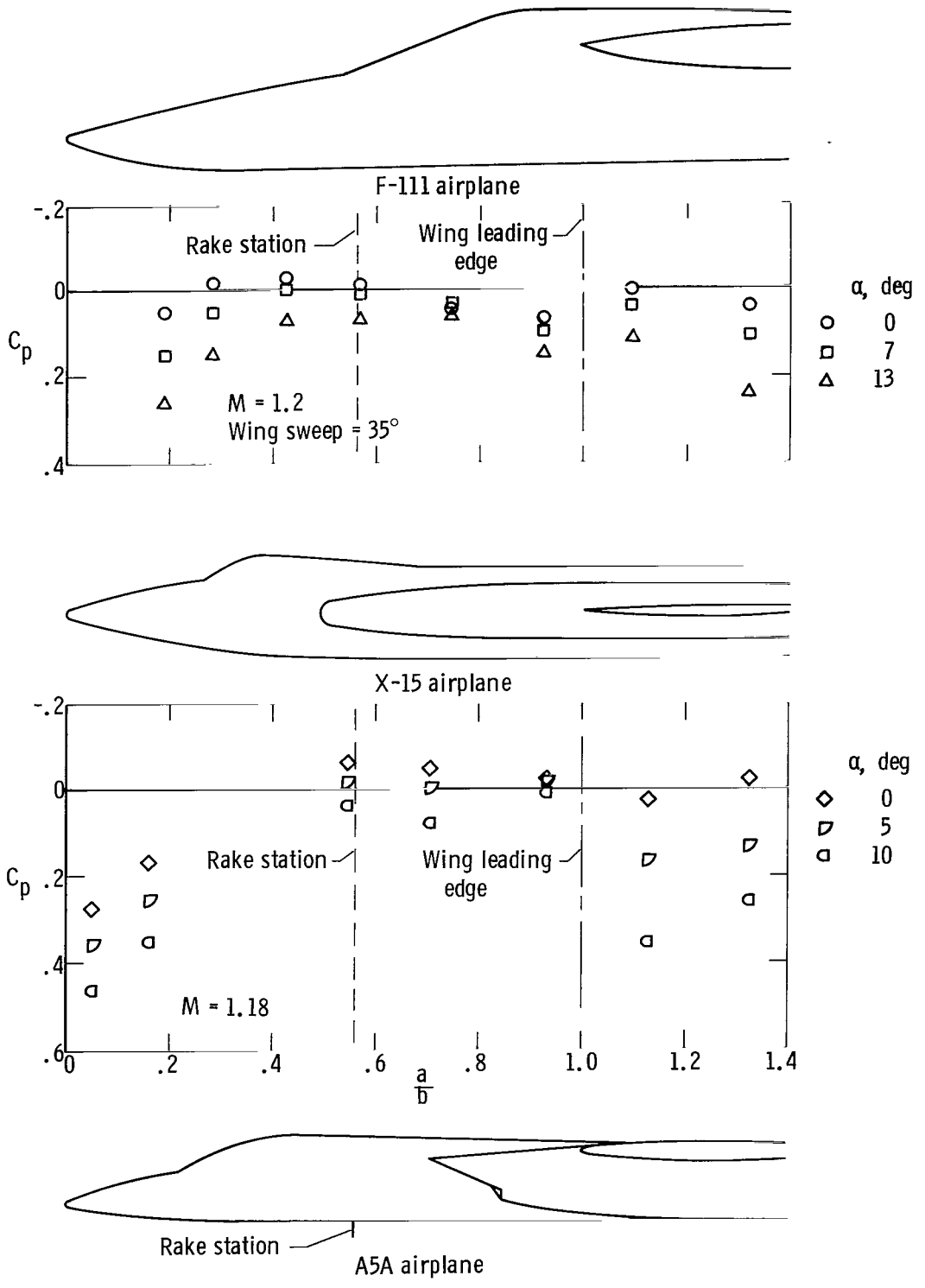

(b) Supersonic.

Figure 5. Concluded.

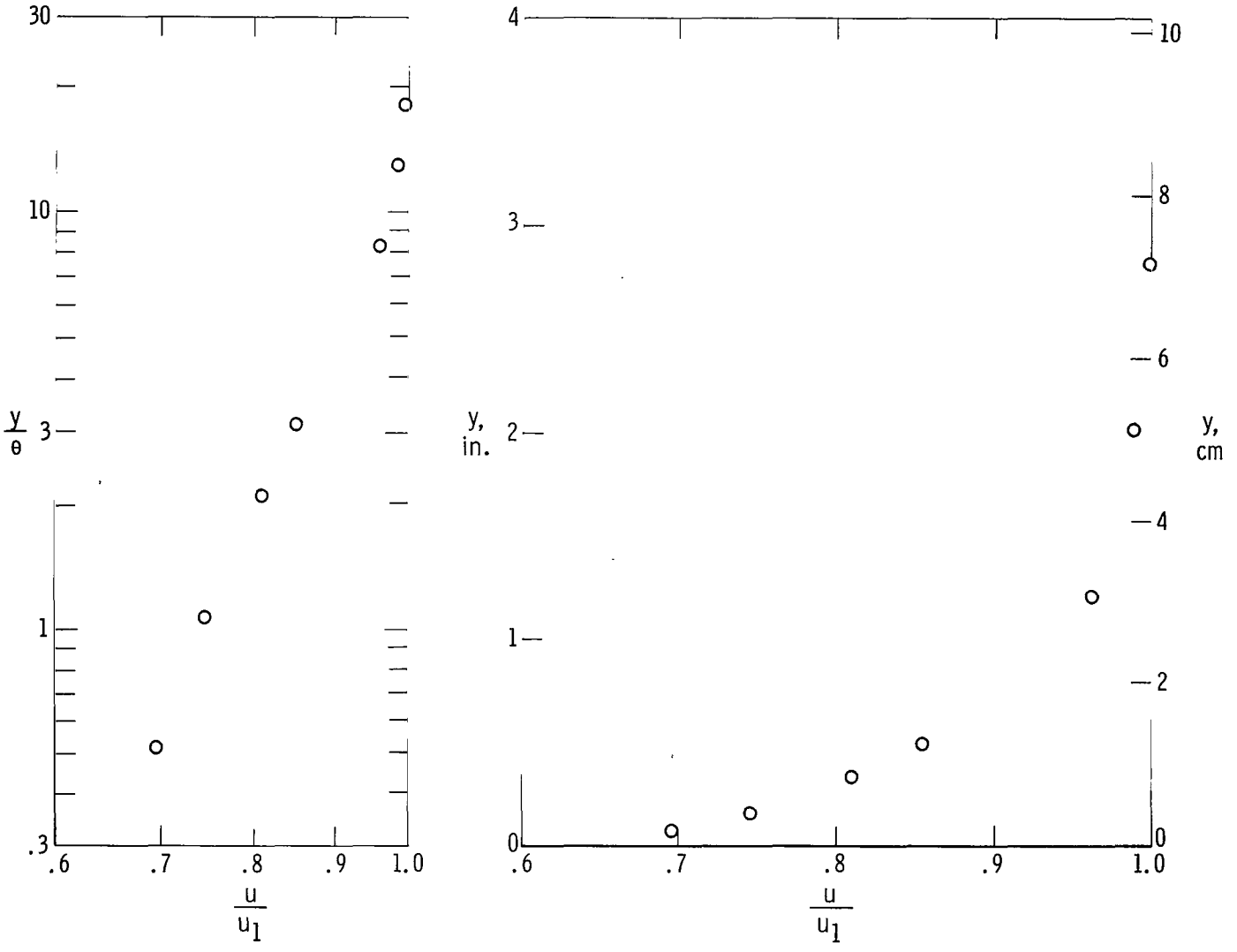

(a) Boundary-layer profile A for $M_1 = 0.51$ and $\alpha = 7.0°$.

Figure 6. Example of boundary-layer profiles obtained in flight.

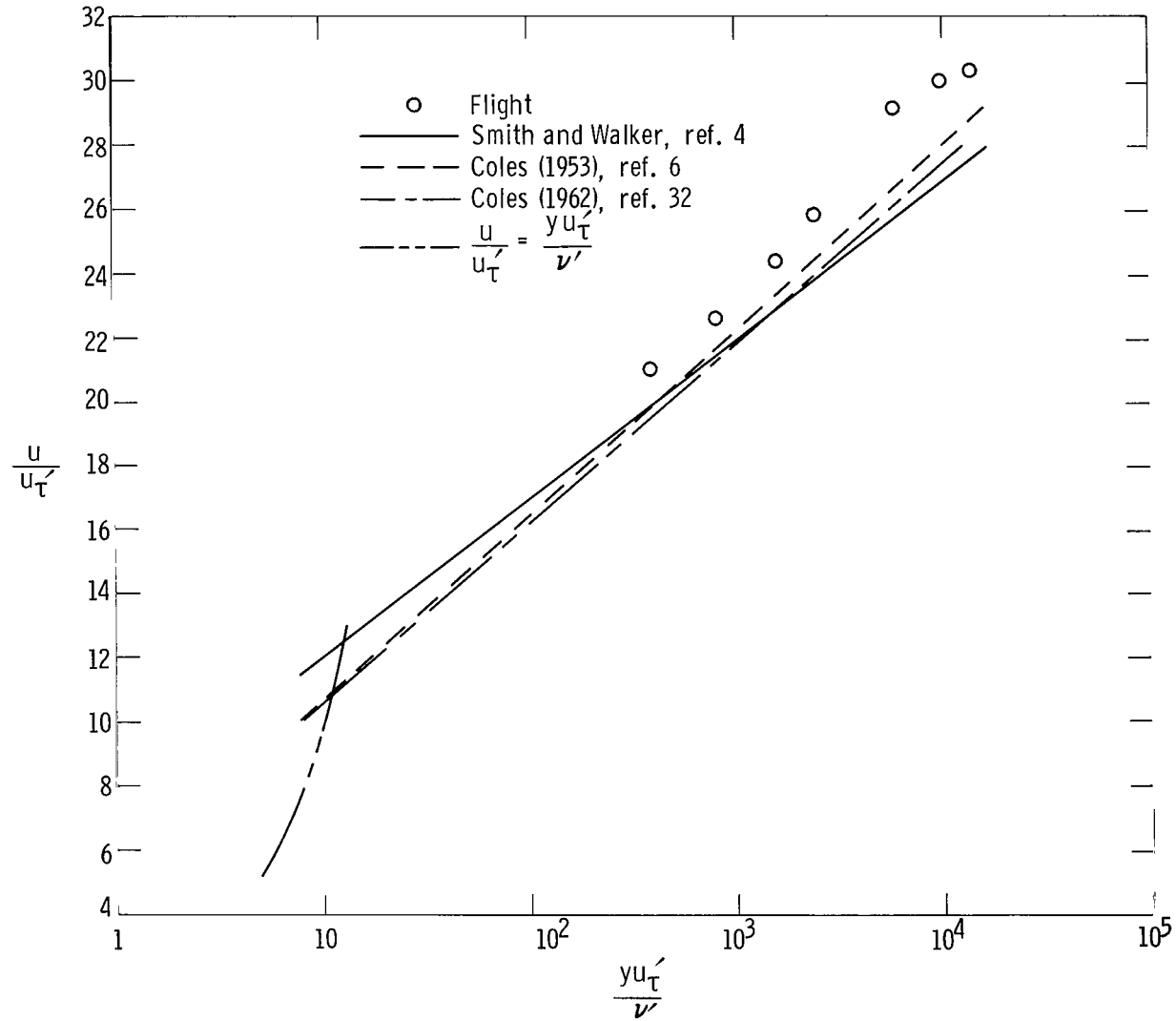

(b) Transformed profile A in terms of wall law, for $M = 0.51$, and $\alpha = 7.0°$.

Figure 6. Continued.

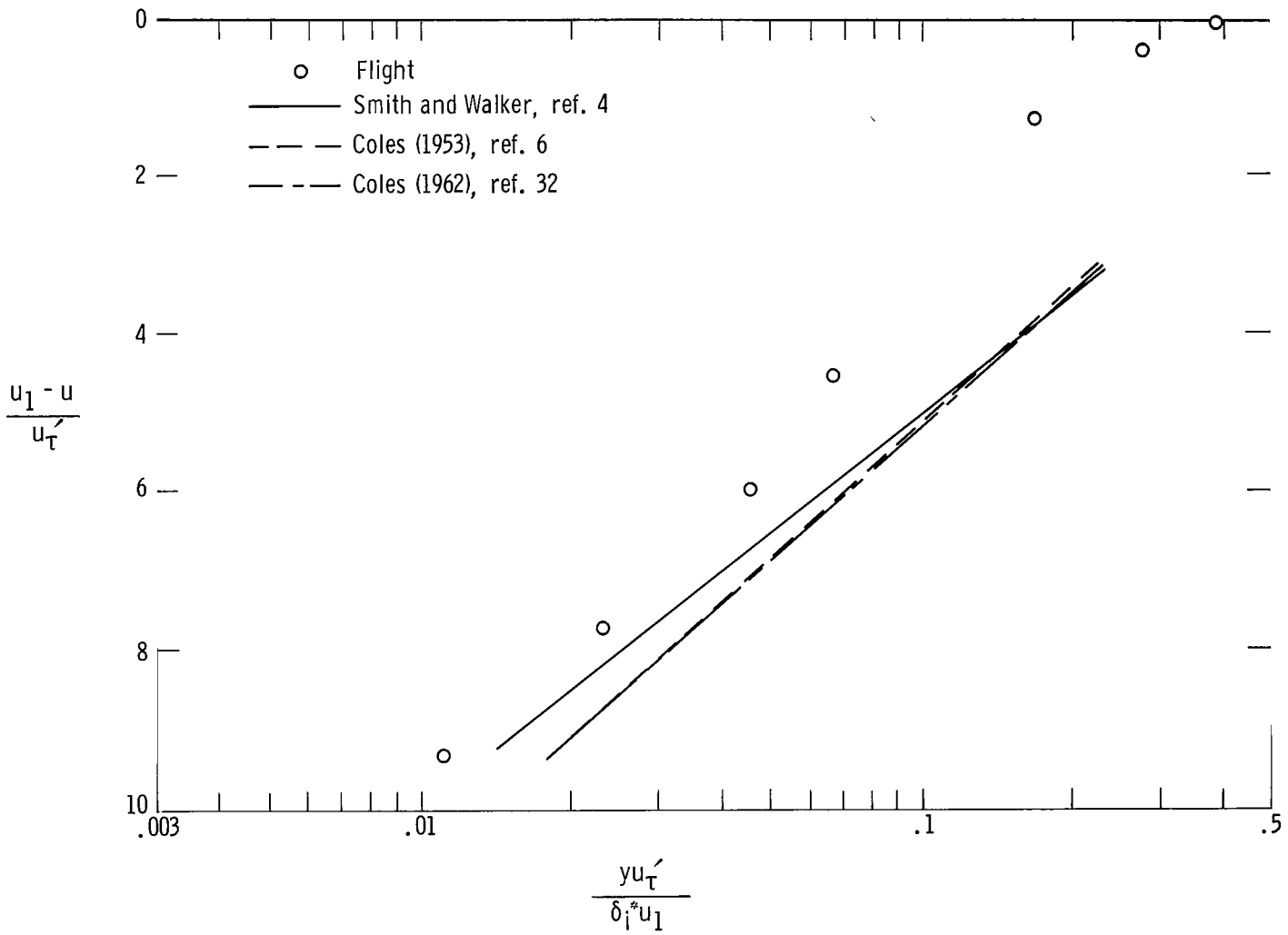

(c) Transformed profile A in terms of defect law, for M = 0.51 and $\alpha = 7.0°$.

Figure 6. Continued.

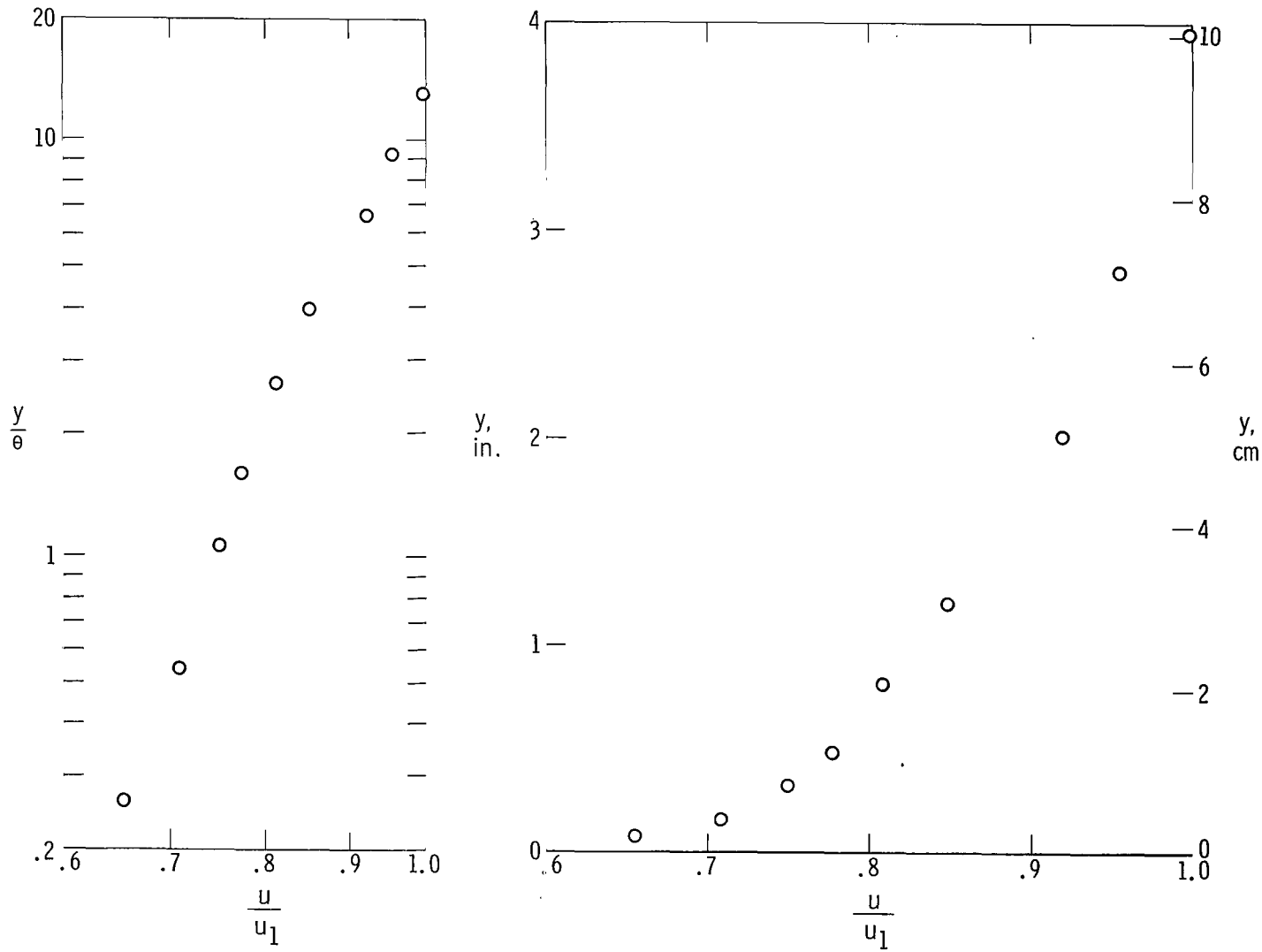

(d) Boundary-layer profile M for $M_1 = 1.54$ and $\alpha \approx 0.1°$.

Figure 6. Continued.

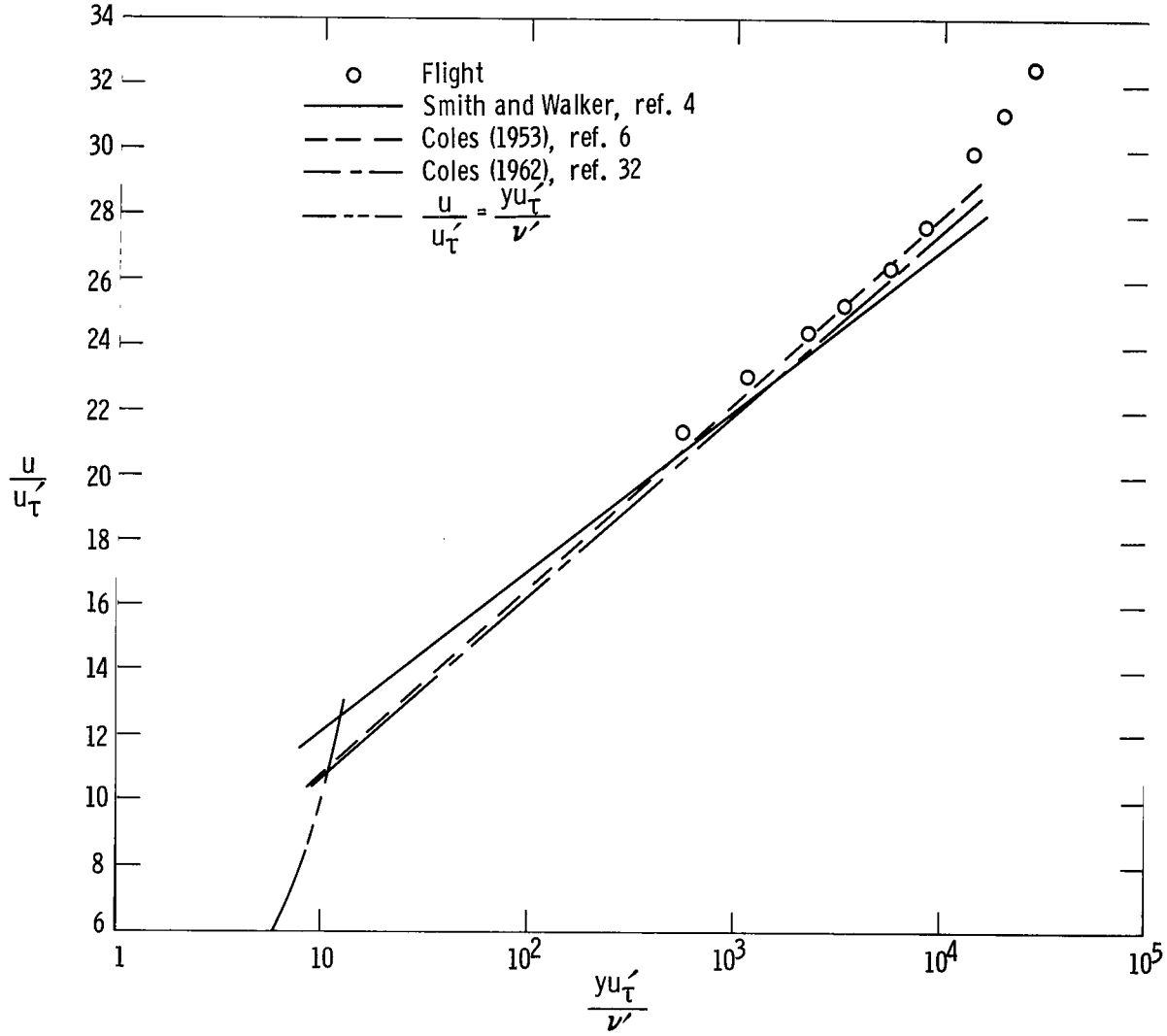

(e) Transformed profile M in terms of wall law, for M = 1.54 and $\alpha \approx 0.1°$.

Figure 6. Continued.

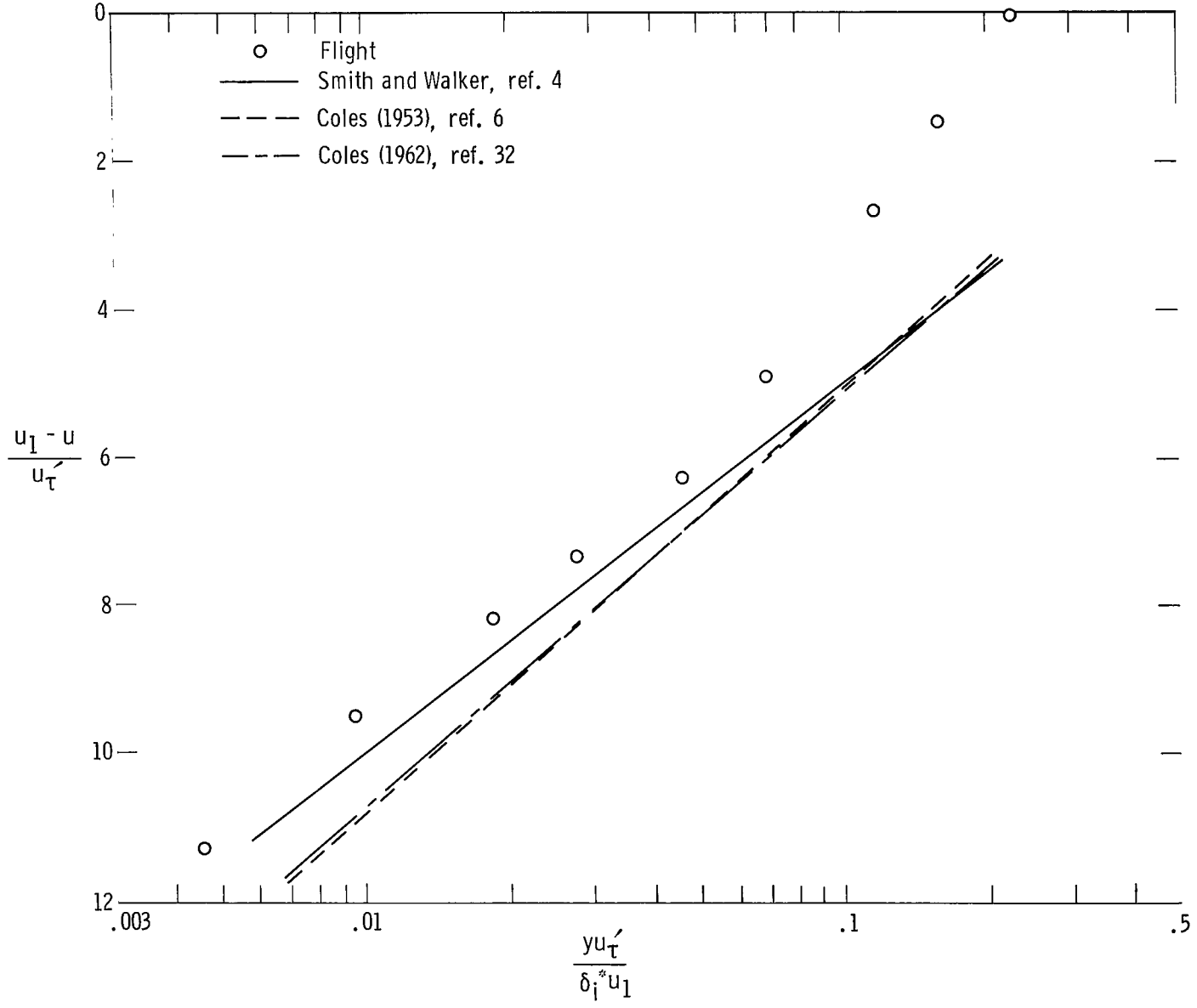

(f) Transformed profile M in terms of defect law, for M = 1.54 and $\alpha \approx 0.1°$.

Figure 6. Concluded.

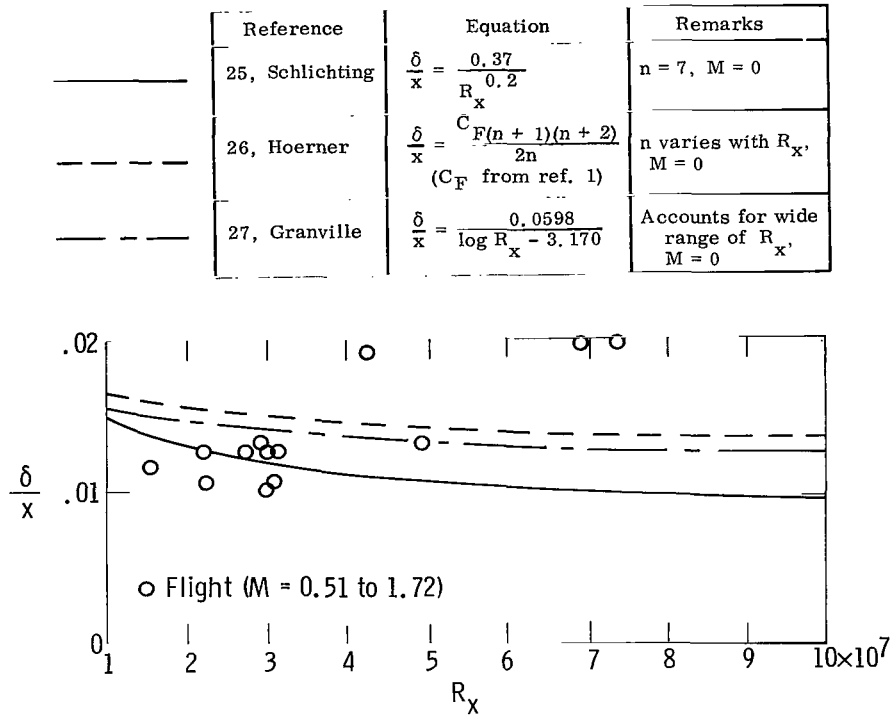

Figure 7. Variation of boundary-layer thickness with Reynolds number. x = 200 in. (508 cm).

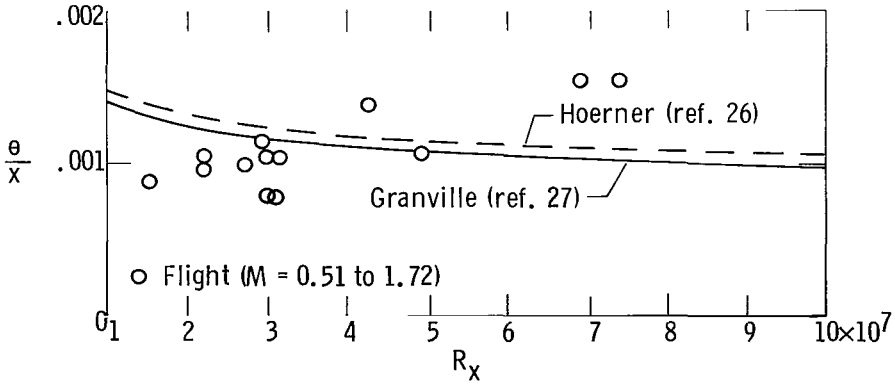

Figure 8. Variation of momentum thickness with Reynolds number. x = 200 in. (508 cm).

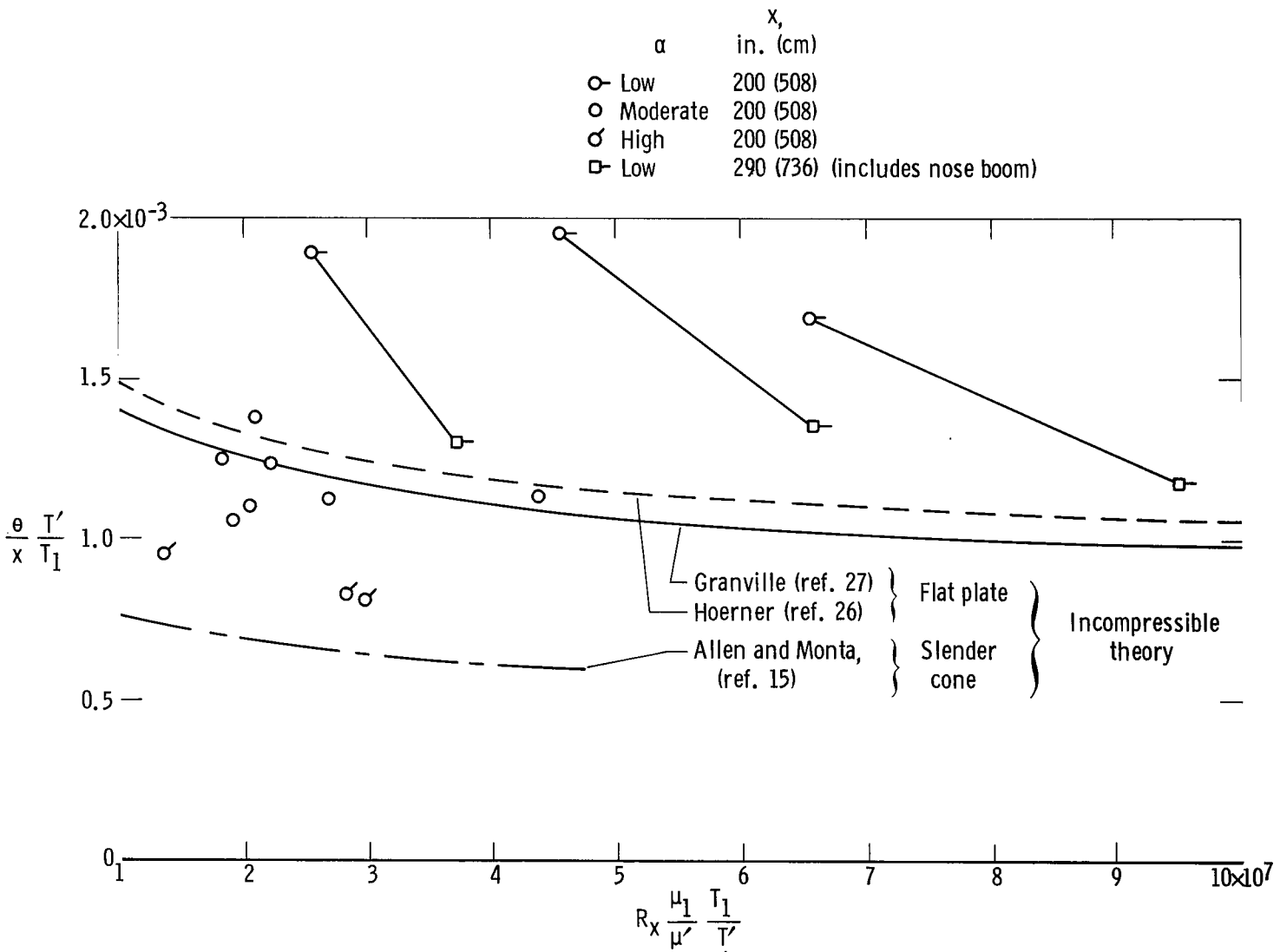

(a) Effect of angle of attack.

Figure 9. Variation of the transformed ratio $\frac{\theta}{x}$ with transformed Reynolds number and comparison with theory.

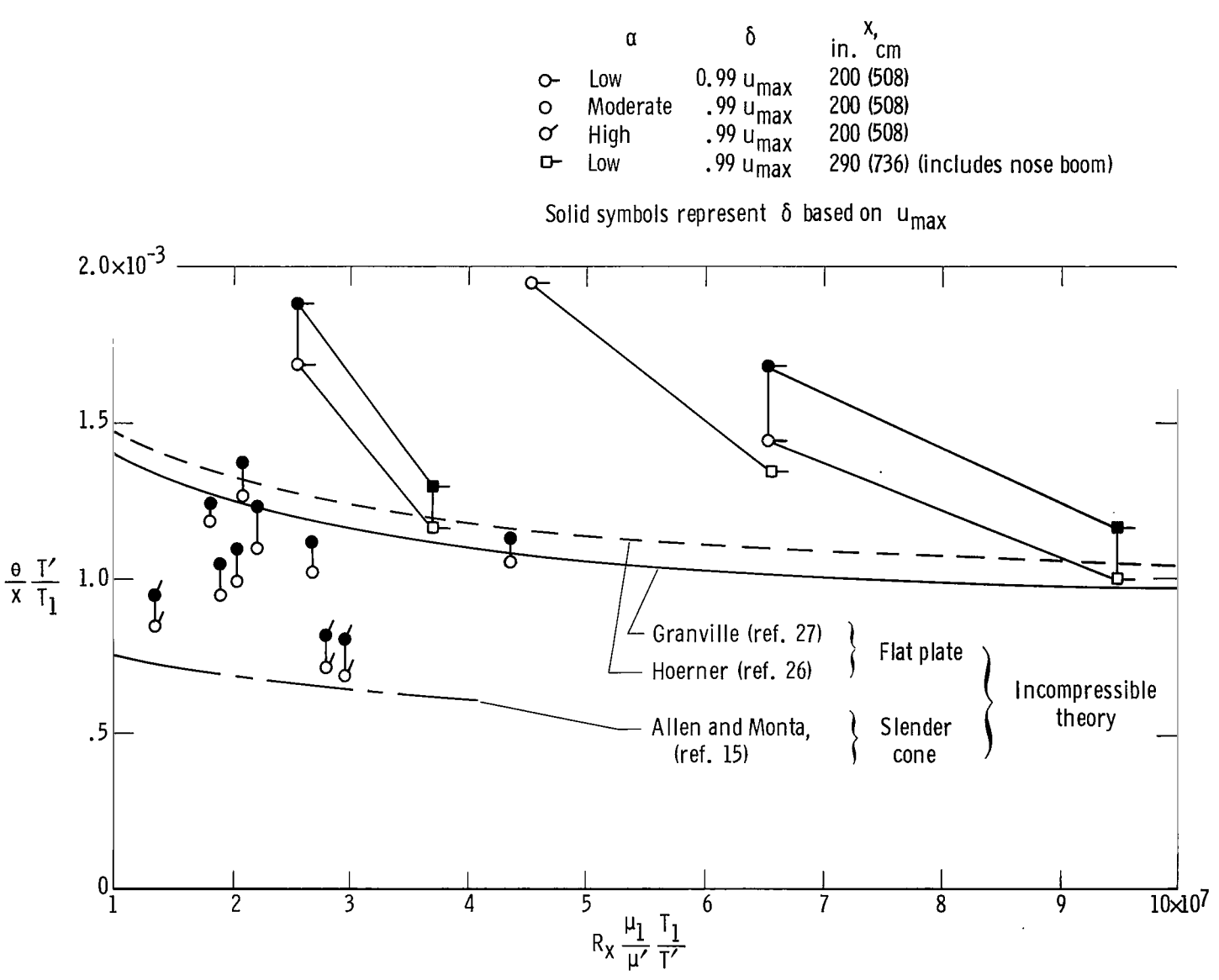

(b) Effect of δ definition.

Figure 9. Concluded.

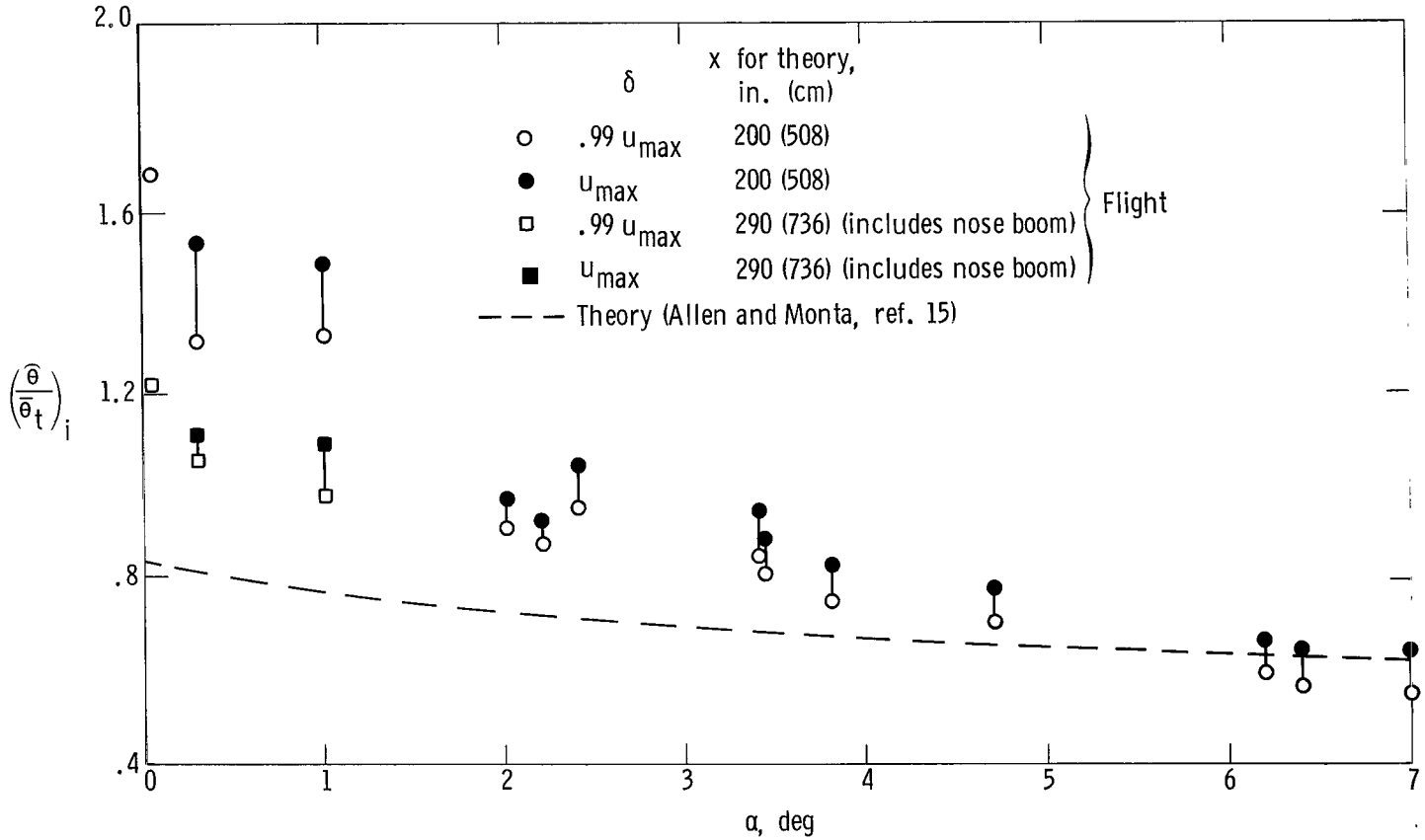

Figure 10. Variation of the momentum-thickness ratio with angle of attack.

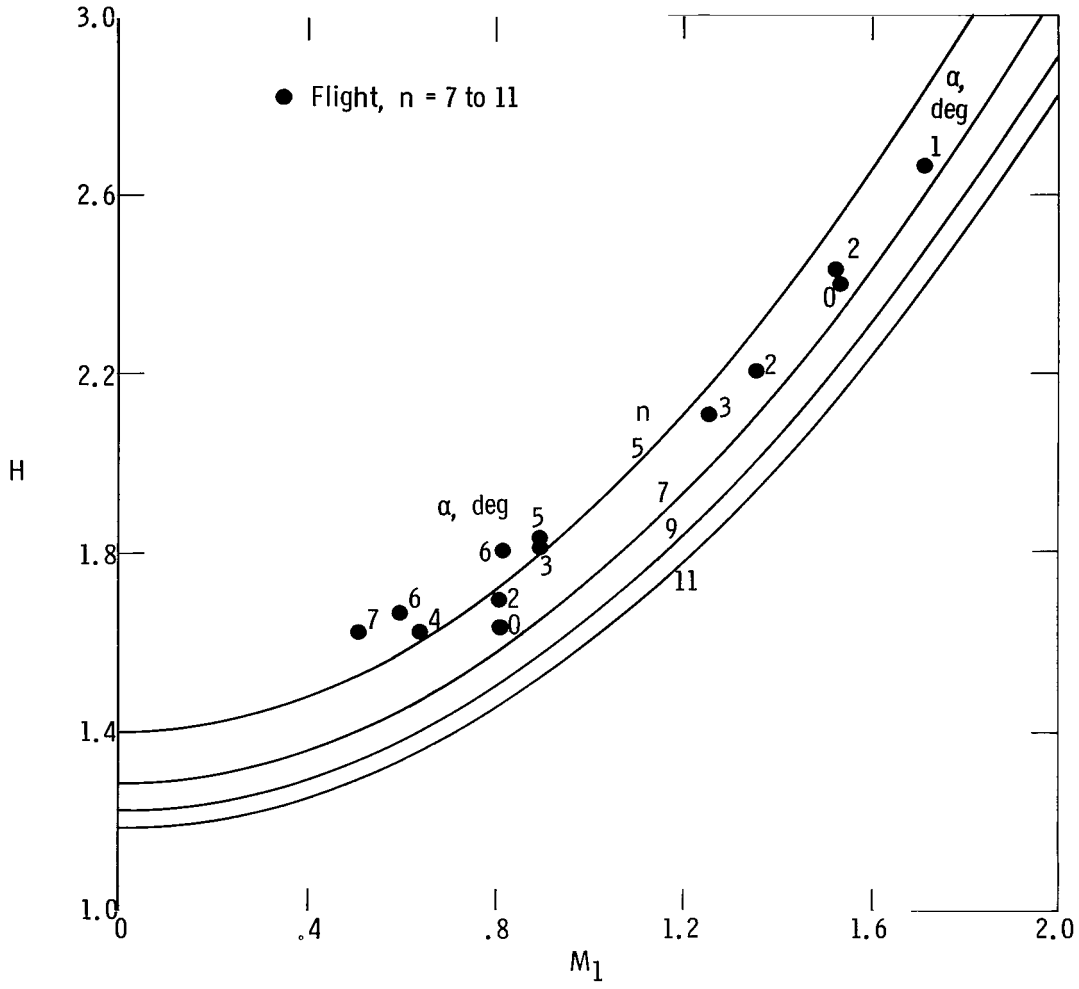

(a) Variation of shape factor with Mach number.

Figure 11. Comparison of shape factors and profile indices obtained from flight with predictions.

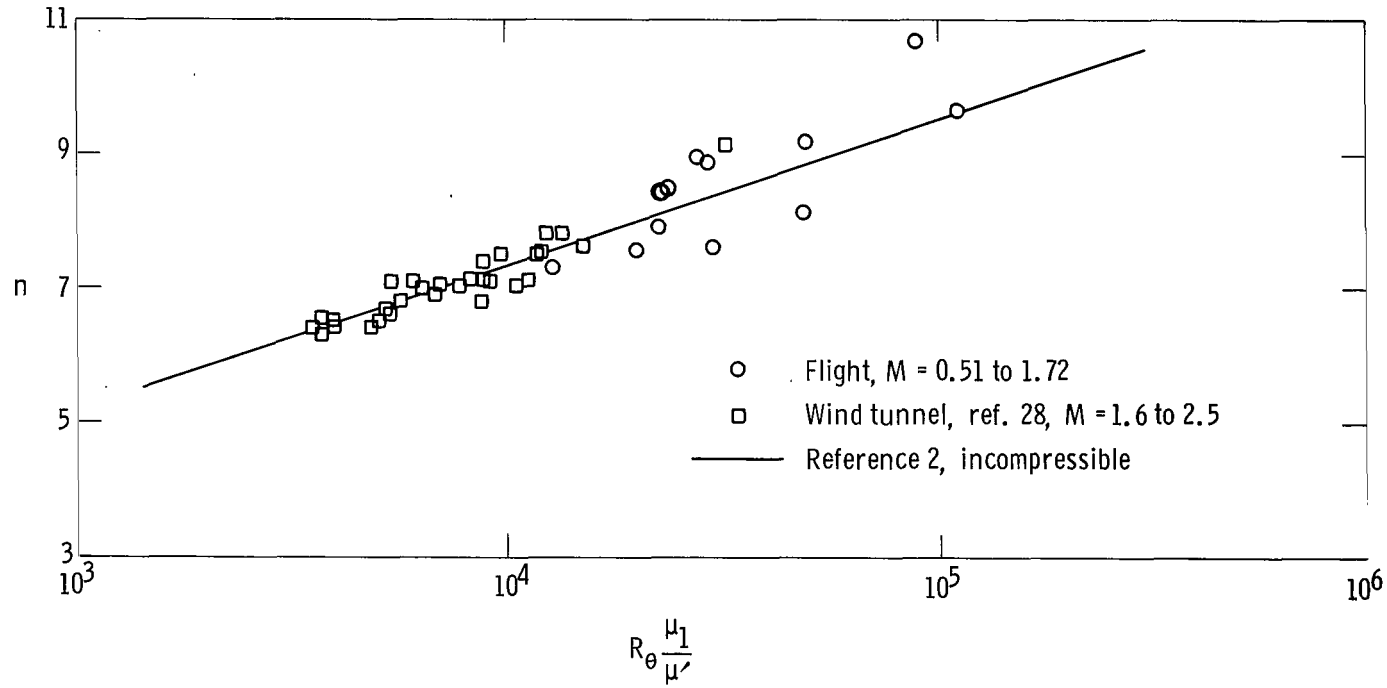

(b) Variation of the boundary-layer-profile index with transformed Reynolds number.

Figure 11. Concluded.

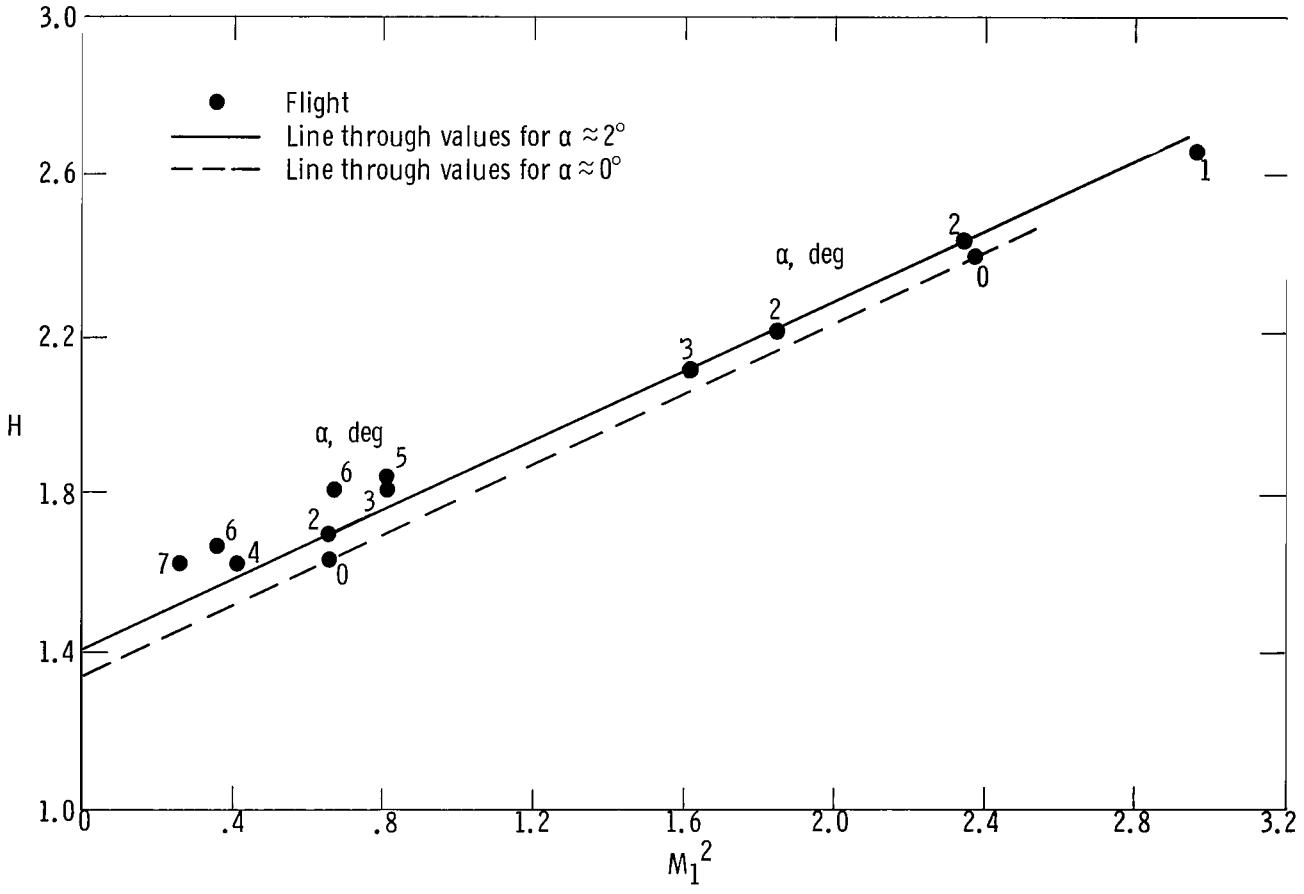

Figure 12. Variation of shape factor with Mach number squared.

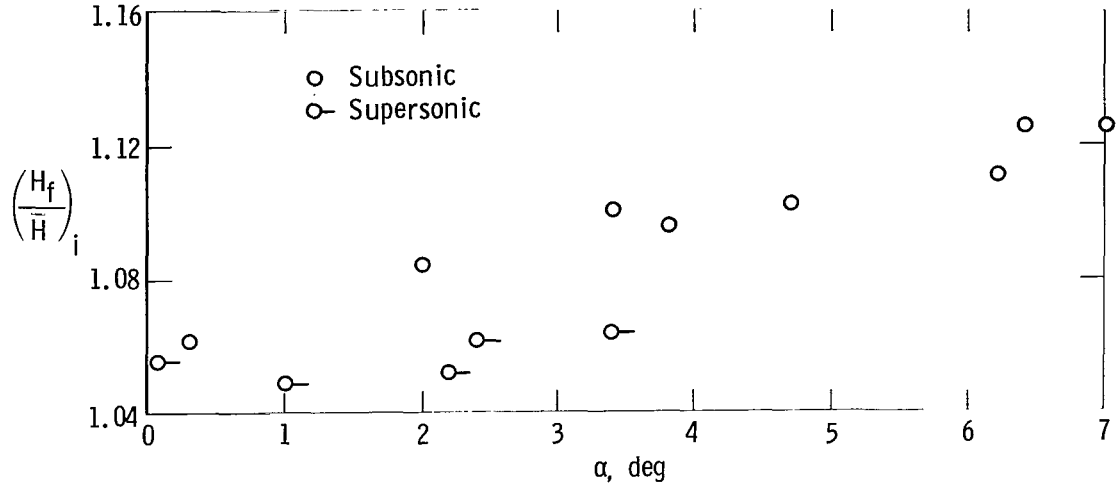

(a) $H_{f_i} = \dfrac{H_f}{(1 + 0.344\ M_1^2)}$.

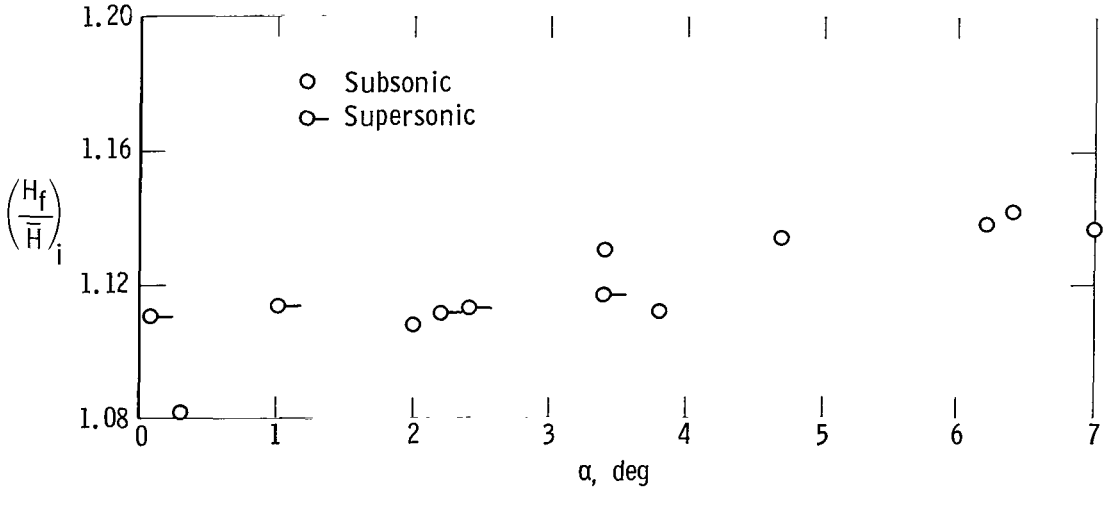

(b) $H_{f_i} = \left[\dfrac{(H_f + 1)}{1 + 0.178\ M_1^2}\right] - 1.$

Figure 13. Variation of the ratio $\left(\frac{H_f}{\bar{H}}\right)_i$ with angle of attack ($\bar{H}_i$ from ref. 4).

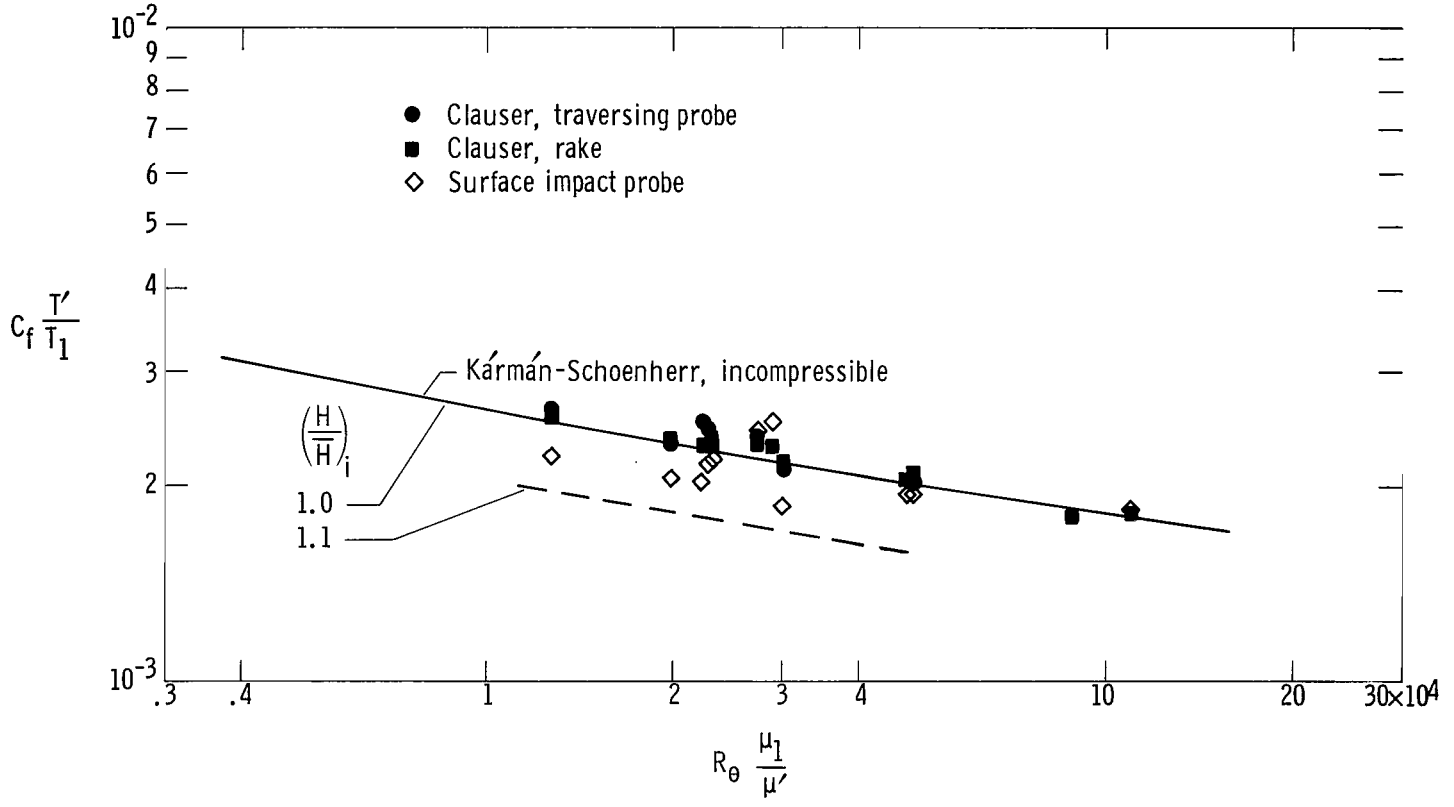

(a) Surface impact probe and the Clauser determination; present study.

Figure 14. Transformed local friction coefficients.

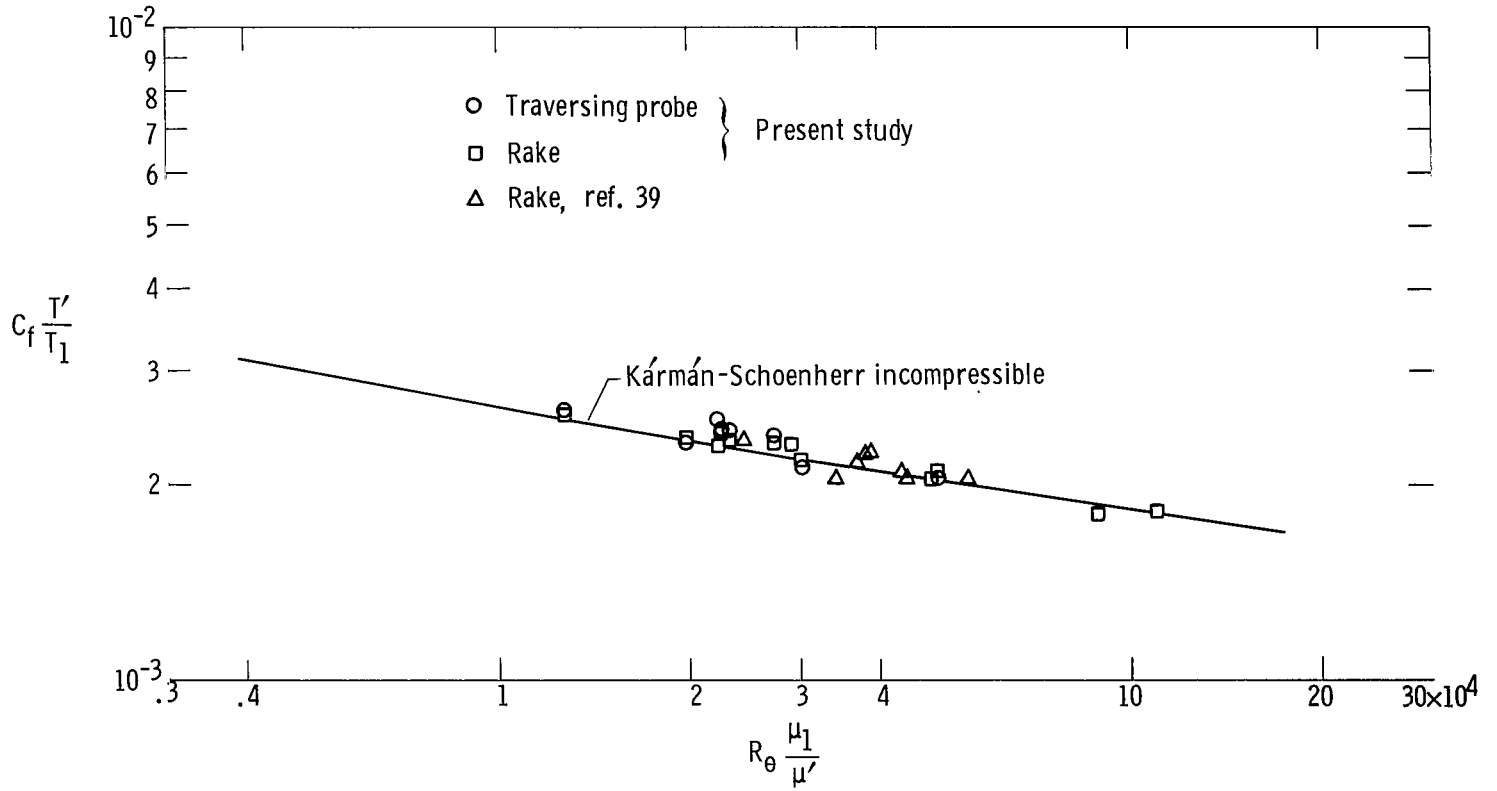

(b) Comparison of Clauser-determined values of the present study with the flight results from reference 39.

Figure 14. Concluded.

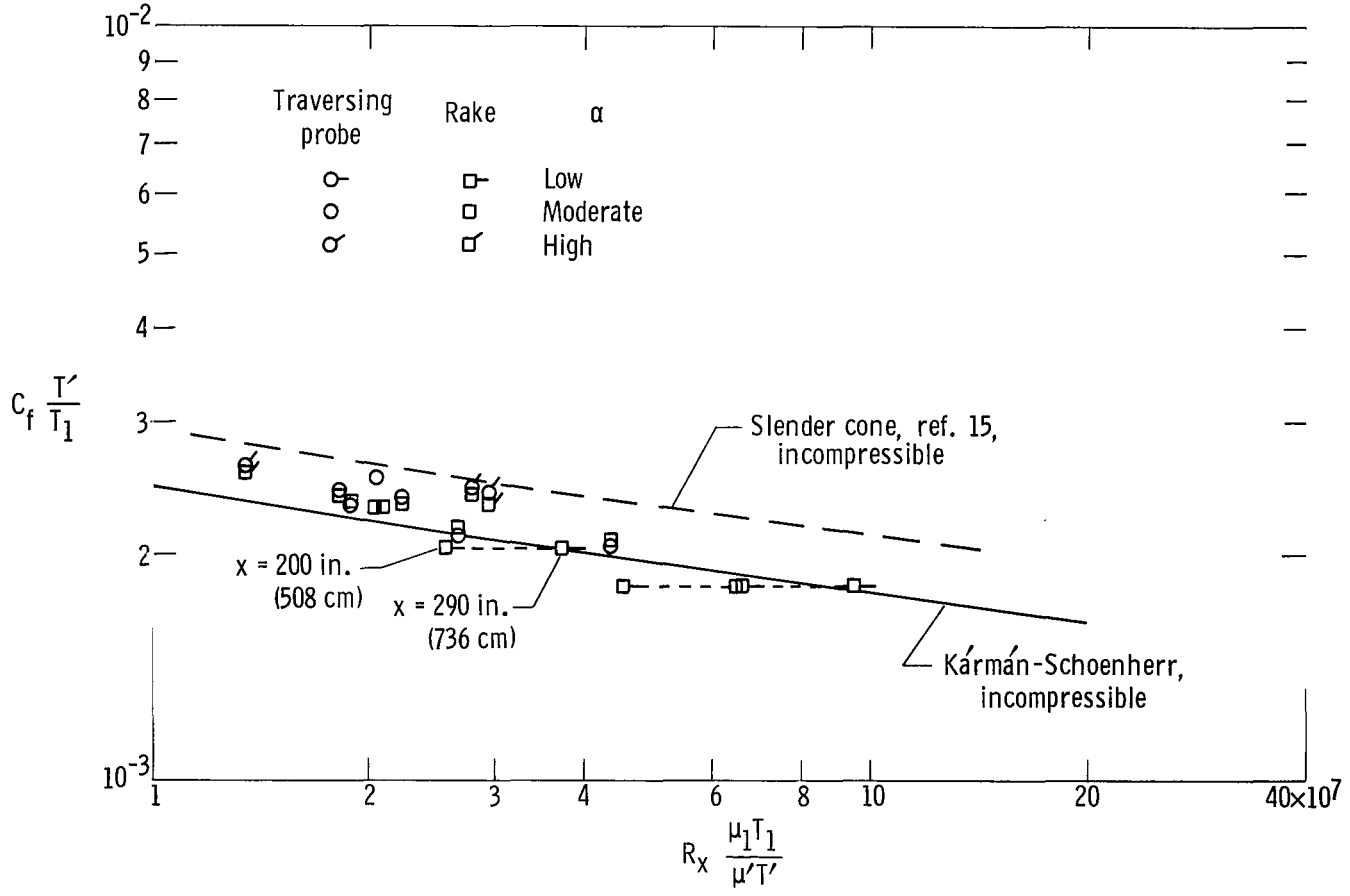

Figure 15. Relationship of transformed Clauser-determined local friction coefficients from flight to incompressible theory for flat plate and slender cone.

"The aeronautical and space activities of the United States shall be conducted so as to contribute . . . to the expansion of human knowledge of phenomena in the atmosphere and space. The Administration shall provide for the widest practicable and appropriate dissemination of information concerning its activities and the results thereof."

—NATIONAL AERONAUTICS AND SPACE ACT OF 1958

NASA SCIENTIFIC AND TECHNICAL PUBLICATIONS

TECHNICAL REPORTS: Scientific and technical information considered important, complete, and a lasting contribution to existing knowledge.

TECHNICAL NOTES: Information less broad in scope but nevertheless of importance as a contribution to existing knowledge.

TECHNICAL MEMORANDUMS: Information receiving limited distribution because of preliminary data, security classification, or other reasons.

CONTRACTOR REPORTS: Scientific and technical information generated under a NASA contract or grant and considered an important contribution to existing knowledge.

TECHNICAL TRANSLATIONS: Information published in a foreign language considered to merit NASA distribution in English.

SPECIAL PUBLICATIONS: Information derived from or of value to NASA activities. Publications include conference proceedings, monographs, data compilations, handbooks, sourcebooks, and special bibliographies.

TECHNOLOGY UTILIZATION PUBLICATIONS: Information on technology used by NASA that may be of particular interest in commercial and other non-aerospace applications. Publications include Tech Briefs, Technology Utilization Reports and Notes, and Technology Surveys.

Details on the availability of these publications may be obtained from:

SCIENTIFIC AND TECHNICAL INFORMATION DIVISION

NATIONAL AERONAUTICS AND SPACE ADMINISTRATION

Washington, D.C. 20546